



HAL
open science

Phytoplankton distribution from Western to Central English Channel, revealed by automated flow cytometry during the summer-fall transition

Arnaud Louchart, Fabrice Lizon, Alain Lefebvre, Morgane Didry, François Schmitt, Luis Felipe Artigas

► To cite this version:

Arnaud Louchart, Fabrice Lizon, Alain Lefebvre, Morgane Didry, François Schmitt, et al.. Phytoplankton distribution from Western to Central English Channel, revealed by automated flow cytometry during the summer-fall transition. *Continental Shelf Research*, 2020, 195, pp.104056. 10.1016/j.csr.2020.104056 . hal-03165188

HAL Id: hal-03165188

<https://amu.hal.science/hal-03165188>

Submitted on 10 Mar 2021

HAL is a multi-disciplinary open access archive for the deposit and dissemination of scientific research documents, whether they are published or not. The documents may come from teaching and research institutions in France or abroad, or from public or private research centers.

L'archive ouverte pluridisciplinaire **HAL**, est destinée au dépôt et à la diffusion de documents scientifiques de niveau recherche, publiés ou non, émanant des établissements d'enseignement et de recherche français ou étrangers, des laboratoires publics ou privés.

Phytoplankton distribution from Western to Central English Channel, revealed by automated flow cytometry during the summer-fall transition

Louchart Arnaud ^{1,*}, Lizon Fabrice ¹, Lefebvre Alain ², Didry Morgane ^{1,3}, Schmitt François G. ¹, Artigas Luis Felipe ^{1,*}

¹ Univ. Littoral Côte D'Opale, Univ. Lille, CNRS, UMR 8187, LOG, Laboratoire D'Océanologie et de Géosciences, F 62930, Wimereux, France

² IFREMER, LER/BL, Boulogne sur Mer, France

³ Aix Marseille Univ., Université de Toulon, CNRS, IRD, MIO, UM110, 13288, Marseille, France

* Corresponding authors : Arnaud Louchart, email address : arnaud.louchart@gmail.fr ; Luis Felipe Artigas, email address : felipe.artigas@univ-littoral.fr

Abstract :

Automated pulse shape-recording flow cytometry was applied to address phytoplankton spatial distribution, at high frequency, in stratified and well mixed water masses in the Western and Central English Channel during the summer-fall transition. Cytometric pulse shapes derived from optical features of single cells allowed the characterization of eight phytoplankton groups. Abundance and total red fluorescence (chlorophyll a autofluorescence) per group were used to define six phytoplankton communities. Their distribution revealed high spatial heterogeneity. Abundance presented a longitudinal gradient for six over the eight groups and succession of brutal shifts along the cruise. Maximum values were often located near the Ushant front in the Western English Channel. A latitudinal gradient characterized the Central English Channel waters under the influence of the Seine estuary. Picophytoplankton (Synechococcus-like cells and picoeukaryotes) represented up to 96% of total abundance and half of the total red fluorescence of the communities near the main front and the Bay of Seine, whereas nanoeukaryotes and microphytoplankton, represented only 4% and less than 1% respectively of total abundance. Both nanoeukaryotes and microphytoplankton dominated the total red fluorescence of the communities of the Central English Channel. The study of traits within each group showed a high variability of traits between communities. The comparison between traits showed that they were independent from each other for some groups (size and red fluorescence per cell for PicoHighFLR and Coccolithophore-like cells; orange and red fluorescence for all the groups), whereas they were dependent for other groups (red fluorescence per cell was dependent of size for picophytoplankton, NanoLowFLR, NanoHighFLR, Cryptophyte-like cells and Microphytoplankton). Variance partitioning revealed that the environmental parameters (temperature, salinity and turbidity) accounted less than spatial descriptors (physical and biological processes) in shaping the communities. Hydrological structures (frontal structures, eddies and tidal streams) were responsible for patches of phytoplankton and defined the structure at the sub-mesoscale (1 – 10 km) in this area.

Highlights

► Automated flow cytometry addresses phytoplankton community changes at high frequency. ► Eight cytometric groups are characterized from pico-to microphytoplankton size range. ► Variation in cytometry-derived traits can be characterized between communities. ► Frontal structures drive phytoplankton spatial distribution at sub-mesoscale.

Keywords : English Channel, phytoplankton distribution, high resolution, automated flow cytometry, fronts, mesoscale structure

52 1. Introduction

53 Carbon uptake and fixation through photosynthesis (Falkowski, 1994; Falkowski et al., 1998; Gregg et
54 al., 2003) make phytoplankton account for up to 50% of the annual global net primary production,
55 while its biomass only represents 2% of the total global biomass (Falkowski et al., 2003; Field et al.,
56 1998). Furthermore, phytoplankton are involved in many biogeochemical cycles (Falkowski, 1994;
57 Falkowski et al., 1998; Gregg et al., 2003) and in most of the marine food webs being a prey for
58 grazers affecting growth, cellular processes and community composition (Holligan and Harbour, 1977;
59 Lampert et al., 1986; Rassoulzadegan et al., 1988). Given the importance of phytoplankton in marine
60 ecosystems, there is a consequent need to perform accurate estimates of abundance and biomass
61 (which are also defined as biological descriptors in the Marine Strategy Framework Directive (MSFD
62 2008/56/EC) and Water Framework Directive (2000/60/EC) in order to understand the populations
63 assembly into different communities and how these communities influence/determine biogeochemical
64 cycles as well as higher trophic levels (*e.g.* Falkowski et al., 1998; Litchman, 2007; Litchman et al.,
65 2007). The large size-range and diversity of phytoplankton characterise high variations of
66 surface/volume ratios as well as physiological capacities, leading to a different capacity of growth
67 among phytoplankton, sometimes dividing twice a day (Alpine and Cloern, 1988). In addition,
68 environmental drivers are often episodic, contributing to quick changes of phytoplankton responses
69 over space and time scales. Current monitoring sampling strategies might fail to detect these responses
70 (Pearl et al., 2007). Therefore, a trade-off in phytoplankton sampling strategies is needed in order to
71 understand the determinism of phytoplankton changes and distribution, considering both fine space
72 and time scales and environmental parameters.

73 Considering the techniques available, the use of microscopy and HPLC pigment analysis provide,
74 respectively, high taxonomical and pigmentary composition. However, they are not suitable for high
75 space and time resolution studies (Cullen et al., 1997; Millie et al., 1997; Richardson and Pinckney,
76 2004) because of the time-consuming and highly specialised work to be carried out back at the
77 laboratory. On the other hand, despite *in vivo* fluorometry could reach a reliable space and time
78 coverage (Rantajärvi et al., 1998), it provides only bulk measurements as estimates of total chlorophyll

79 *a* (as a proxy of phytoplankton biomass). Several innovative techniques (*e.g.* multispectral
80 fluorometry, automated flow cytometry, remote sensing) have shown to give representative insights
81 into phytoplankton composition (at least at the functional level), abundance and/or chlorophyll *a* at
82 high resolution (Bonato et al., 2015; De Monte et al., 2013; Lefebvre and Poisson-Caillault, 2019;
83 Marrec et al., 2018, 2014; Thyssen et al., 2015). Among these techniques, automated “pulse shape-
84 recording” flow cytometry (PSFCM) addresses almost the whole phytoplankton size-range (c.a. from
85 less than 1µm to 800 µm width) at single-cell or single-colony level and characterizes them based on
86 their combined or integrated optical properties (*i.e.* light scattering, fluorescence; Dubelaar et al.,
87 2004, 1999). Indeed, this technique records the entire pulse shape of a single particle (Rutten et al.,
88 2005; Thyssen et al., 2008b, 2008a), from small cells as *Prochlorococcus*-like (Marrec et al., 2018) up
89 to large cells and/or colonies of diatoms or *Phaeocystis globosa* (Bonato et al., 2016, 2015; Rutten et
90 al., 2005). Moreover, the cytometric optical properties provide useful proxies of cell length, width,
91 morphology, internal composition and physiology which can be assimilated to functional derived
92 traits. Therefore, the variation of phytoplankton traits at high frequency remain to be investigated
93 across the different spatial scales.

94 The Western and Central part of the English Channel are well-documented areas which benefit from
95 sustained monitoring (*e.g.* Astan Buoy, Astan & Estacade SOMLIT stations, L4 and E1 stations;
96 Eloire et al., 2010; Goberville et al., 2010; Not et al., 2004; Smyth et al., 2010; Sournia et al., 1987).
97 This epicontinental sea is strongly impacted by climate variability (Goberville et al., 2010) making
98 seasonal and interannual variation in the hydrological and climatic conditions responsible of changes
99 in plankton communities composition (Foulon et al., 2008; Marie et al., 2010; Tarran and Bruun,
100 2015; Widdicombe et al., 2010). In the Western English Channel (WEC), from May to October, the
101 hydrological conditions go from well-stratified to well-mixed conditions and shape the position of the
102 Ushant tidal front (Pingree and Griffiths, 1978). Eddies that bring high nutrient concentrations in
103 addition to the light, make communities accumulating along the front, especially diatoms and
104 dinoflagellates, and contribute to high biomass (Landeira et al., 2014; Pingree et al., 1979, 1978,
105 1977). Moreover, the geostrophic flow, eddies, wind upwelling and tidal streams occur along the front

106 allowing phytoplankton dispersion and crossing the front (Pingree et al., 1979). Therefore, the front
107 extends on scales from meters to kilometres (d'Ovidio et al., 2010; Ribalet et al., 2010). In the Central
108 English Channel (CEC), both the English and the French coast are influenced by river run-off. In the
109 French part, the Seine River contributes to form permanent halocline stratification (Brylinski and
110 Lagadeuc, 1990; Menesguen and Hoch, 1997). During the late summer-fall period, the Bay of Seine is
111 initially characterised by high abundance of diatom (Jouenne et al., 2007). Then, when the depletion of
112 nutrient occurs in summer, diatom abundance decrease and dinoflagellate abundance increase (Thorel
113 et al., 2017). Along the English coast, the Southampton Water estuarine system contributes largely to
114 enhance nutrients along the coast (Hydes and Wright, 1999). Nutrients are especially brought by the
115 Test and Itchen rivers, which drain agricultural land as well as sewage discharge effluents (Hydes and
116 Wright, 1999) resulting in chlorophyll *a* peaks in spring and summer (Iriarte and Purdie, 2004; Kifle
117 and Purdie, 1993; Leakey et al., 1992).

118 Despite most of phytoplankton studies in the English Channel concerned the coastal areas (*e.g.* Hydes
119 and Wright, 1999; Iriarte and Purdie, 2004; Jouenne et al., 2007; Marie et al., 2010; Not et al., 2004;
120 Pannard et al., 2008; Smyth et al., 2010; Tarran and Bruun, 2015; Widdicombe et al., 2010), some of
121 them concerned coastal-offshore gradients focusing both in the Eastern English Channel (EEC, Bonato
122 et al., 2016, 2015; Lefebvre and Poisson-Caillault, 2019), Central English Channel (WEC, Napoléon
123 et al., 2014, 2012) and Western English Channel (Garcia-Soto and Pingree, 2009; Marrec et al., 2014,
124 2013; Napoléon et al., 2013) (Garcia-Soto and Pingree, 2009; Marrec et al., 2014, 2013; Napoléon et
125 al., 2014, 2013, 2012). Some attempts were carried out on transects crossing the English Channel in
126 the WEC and CEC (Garcia-Soto and Pingree, 2009; Marrec et al., 2014, 2013; Napoléon et al., 2013).
127 However, these studies reflected three major drawbacks: first of all, some transects were carried out
128 along a latitude gradient, missing the longitude component in which spatial gradients are particularly
129 known to occur in the English Channel (Napoléon et al., 2014, 2013, 2012). Secondly, most of them
130 resulted in a spatial aliasing by missing any fine spatial scale variability. Finally, these spatiotemporal
131 studies mainly sampled the largest organisms ($> 20 \mu\text{m}$) of the phytoplankton compartment, missing
132 most of the picophytoplankton and the small nanophytoplankton ($< 20\mu\text{m}$) fraction.

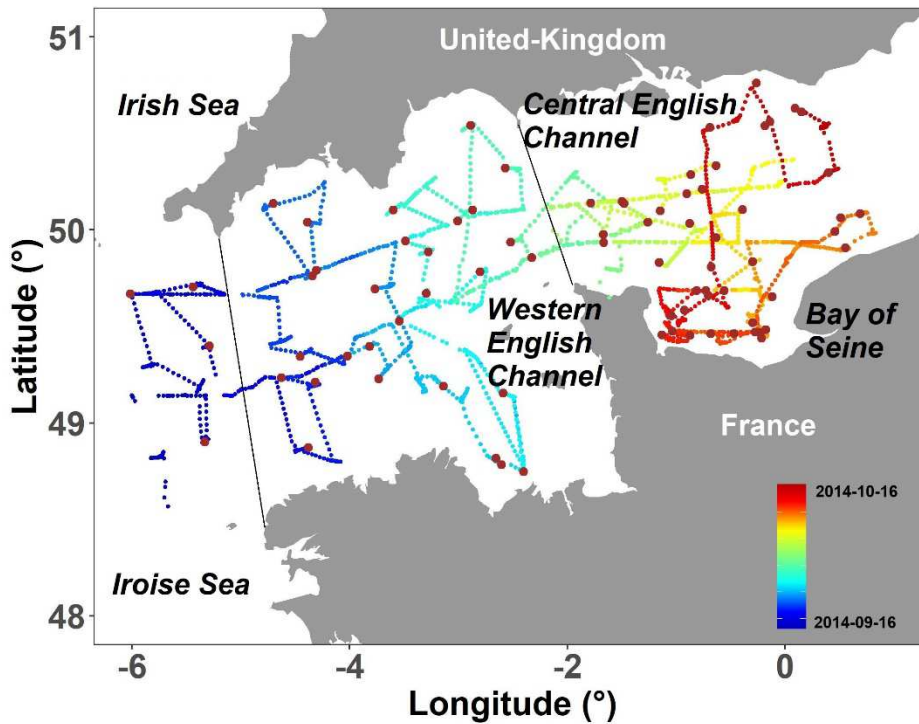
133 In the present study, we analyse the spatial distribution of some phytoplankton size- and optically-
134 defined functional groups as well as their assembly in communities, highlighting the relation between
135 environmental and spatial features with phytoplankton communities' variability, addressed at high
136 frequency, on a high spatial sampled gridded area. Phytoplankton single-cells and colonies were
137 characterised by continuous recording of sub-surface pumped seawater, by using an automated "pulse
138 shape-recording" flow cytometer coupled to continuous recording hydrological features. With a high
139 resolution spatial sampling strategy, our aims were: (i) to study the phytoplankton distribution per
140 functional group and the variation of the traits within each group across space with respect to meso- to
141 sub-mesoscale hydrological features as frontal areas (ii) to identify the key environmental and spatial
142 variables that could explain the variability between communities' composition and (iii) to define the
143 scale of variability of phytoplankton communities among sites.

144 2. Materials and methods

145 2.1 Cruise outlines

146 Samples were collected during a multidisciplinary cruise focusing on an ecosystemic end-to-end
147 approach of fisheries in the Western English Channel. The CAMANOC (CAMPagne MANChe
148 OCcidentale, Travers-Trolet and Verin, 2014) cruise took place on board the RV *Thalassa* (Ifremer)
149 from the 16th of September to the 16th of October 2014, during the summer-fall transition. The ship
150 crossed the English Channel from West to East (Fig. 1). A Pocket-FerryBox system (PFB, 4H-JENA)
151 was coupled to a pulse shape-recording flow cytometer (PSFCM, CytoSense, Cytobuoy), a
152 thermosalinometer (SeaBird SBE21) and an *in vivo* fluorometer (Turner Designs 10-AU). *In vivo*
153 fluorometer required a two steps calibration. The first one used a blank water (de-ionized water) and
154 the second one used a solid standard. The water intake was at the front of the ship's cooling system at
155 a fixed depth (4 m), and in normal ship operation seawater is constantly pumped. The PFB was
156 assembled with sensors for salinity and temperature (Seabird 45 micro TSG), and turbidity (Seapoint).
157 Seawater was pumped at 4 m depth and was continuously analysed by all the sensors. The acquisition
158 of data was continuously performed, and we obtained an integration of the measurement from 1
159 minute (PFB) to 10 minutes (PSFCM). Because of a relatively brief transit time of water from the
160 water intake to PFB, the observations are representative of sub-surface conditions. The lower
161 resolution was kept to merge phytoplankton functional features with environmental data. The ship
162 navigated at the speed of 11 knots for 1 month. This led to a resolution of approximately 3.4 km (for
163 automated flow cytometry) with a total of 2910 samples, considering stops for discrete fisheries,
164 benthos, plankton and hydrological sampling.

165



166

167 Figure 1: Continuous recording every 10 minutes by a pulse shape-recording flow cytometer (PSFCM)
 168 during the CAMANOC cruise from Sept. 16th (blue dots) to Oct. 16th (red dots) and 78 discrete (CTD)
 169 stations (brown dots). Dashed lines correspond to geographical separation of the main regions: Celtic
 170 Seas (including Irish and Iroise Sea), Western English Channel and Central English Channel.

171

172 2.2 Stratification and mixing of water masses

173 CTD (Seabird SBE 21) casts (78) were performed during the cruise. Temperature (°C), salinity,
 174 density ($\text{kg}\cdot\text{m}^{-3}$) and depth (m) were recorded at a rate of 1 measure per second. We used the density
 175 from the CTD casts to calculate the squared of buoyancy frequency, N^2 (s^{-2} ; 3), in order to quantify the
 176 vertical density gradient throughout the water column which quantifies the stratification:

$$177 \quad (3) \quad N^2 \equiv g/\rho_0 \times (\delta\rho(z) / \delta z)$$

178 where g ($\text{m}\cdot\text{s}^{-2}$) is the acceleration due to gravity, ρ_0 ($1026 \text{ kg}\cdot\text{m}^{-3}$) is seawater reference density,
 179 $\delta\rho$ ($\text{kg}\cdot\text{m}^{-3}$) is the density differential along the water column and δz is the depth of the water column,
 180 between surface and bottom.

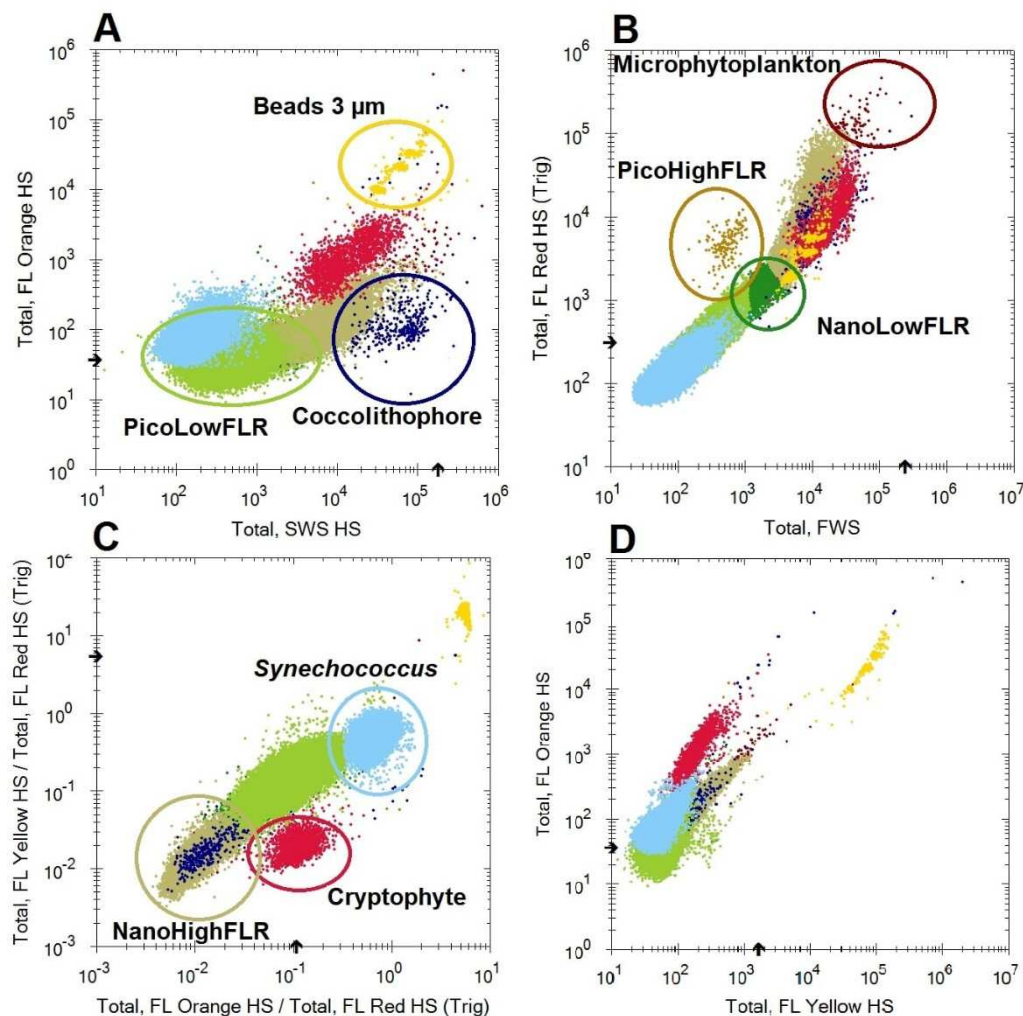
181 2.3 Plankton analysis

182 Continuous pumped waters as well as discrete samples were analysed by a CytoSense (Cytobuoy b.v.,
183 Netherlands), an automated flow cytometer (FCM) with the ability of recording the entire optical pulse
184 shape of each particle (“pulse shape-recording flow cytometer”: PSFCM). Five signals compose a
185 particle optical profile. The forward scatter (FWS) is collected via a PIN photodiode whereas the
186 sideward scatter (SWS) and three types of fluorescence: red fluorescence (FLR: 668-734 nm), orange
187 fluorescence (FLO: 604-668 nm) and yellow fluorescence (FLY: 536-601 nm) are collected via a
188 photomultiplier. The instrument uses a solid-state laser (Coherent Inc, 488 nm, 50 mV) to analyse,
189 count and characterise single-cells and colonies (Dubelaar et al., 2004; Pomati et al., 2013; Pomati and
190 Nizzetto, 2013) from 1 μm to 800 μm width and a few mm length (Dubelaar et al., 1999). Each
191 particle passes through a 5 μm laser beam at a speed of 2 m s^{-1} . A trigger-level was used on the red
192 fluorescence (FLR) in order to separate phytoplankton and non-fluorescent particles (Thyssen et al.,
193 2015). Continuous recording was performed with this configuration and the trigger-level was set at 15
194 mV during 9 min at a flow rate of 4.5 $\mu\text{L s}^{-1}$. The clustering was performed manually with the
195 CytoClus software (Cytobuoy b.v., www.cytobuoy.com). The determination of each group was
196 processed considering the amplitude and the shape of the five signals, referring also to previous work
197 on automated flow cytometry in this area (Bonato et al., 2016, 2015; Thyssen et al., 2015) and
198 according to bead size calibration. In addition, the CytoClus software provides several statistical
199 features on each signal (*e.g.* Length, Total, Average...) as well as the distribution of the different
200 populations of events. The length of the FWS was used as a proxy for cell size. A standardisation of
201 each particle from each cluster was carried out with calibrated beads of 3 μm . Two thresholds were set
202 up: the first around 3 μm in order to separate picoeukaryotes from nanoeukaryotes and the second
203 around 20 μm in order to separate nanoeukaryotes from microphytoplankton. A group was named
204 according to its estimated size and to its pigmentary features. Following Bonato et al. (2015) particle
205 size was corrected with the measured length FWS of the beads (1 & 2).

206 (1) Correction factor = real beads size / Measured beads size

207 (2) Estimated particles size (μm) = Measure particles size \times Correction factor

208 Based on the common vocabulary for automated FCM (available at <https://www.seadatanet.org>), we
 209 characterised 6 main functional groups by automated flow cytometry: *Synechococcus*-like cells,
 210 picoeukaryotes, nanoeukaryotes, Cryptophyte-like cells, Coccolithophore-like cells and
 211 Microphytoplankton. In addition, sub-groups were characterised within the picoeukaryotes and
 212 nanoeukaryotes groups, according to their red fluorescence's level. Finally, we defined three
 213 picophytoplankton groups (<3 μ m): *Synechococcus*-like cells, PicoLowFLR, PicoHighFLR; four
 214 nanoeukaryotes groups (3 to 20 μ m): Cryptophyte-like cells, Coccolithophore-like cells, NanoLowFLR
 215 and NanoHighFLR; and one microphytoplankton group (>20 μ m; Fig. 2).



216

217 Figure 2: Cytograms allowing the characterisation of different phytoplankton groups. (A) Total
 218 Orange Fluorescence (TFLO) vs. Total Sideward Scatter (Total SWS). (B) Total Red Fluorescence
 219 (TFLR) vs. Total Forward Scatter (Total FWS). (C) Ratio of Total Yellow Fluorescence over Total

220 Red Fluorescence and Total Orange Fluorescence over Total Red Fluorescence
221 (TFLY/TFLR)/(TFLO/TFLR). (D) Total Orange Fluorescence (TFLO) vs. Total Yellow Fluorescence
222 (TFLY). Clusters of single, doubles and triples of beads of 3 μm are merged here.

223 **2.4 Statistical analysis and mapping**

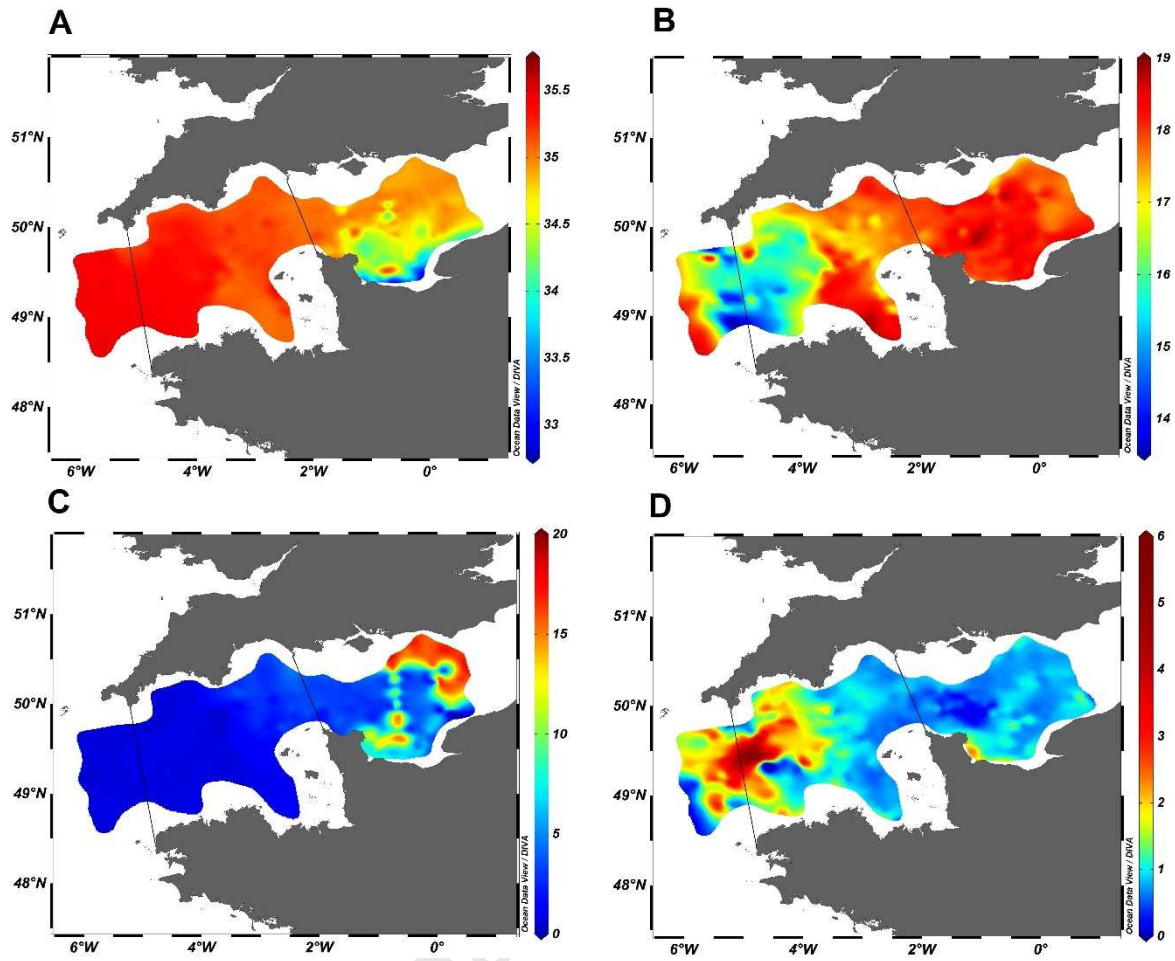
224 We considered the environmental parameters (*i.e.* temperature, salinity and turbidity) and *in vivo* total
225 fluorescence obtained either by the thermo-salinometer (temperature and salinity), the PFB (turbidity)
226 and the Turner fluorometer (*in vivo* total fluorescence) to compute a hierarchical classification analysis
227 based on Euclidean distance. A hierarchical classification was computed also for cytometric groups,
228 separately, to characterize the similarity between the phytoplankton communities among the sites. We
229 used scaled data to detect the similarity among the relative changes in community composition, and
230 we computed the Jaccardized Czekanowski similarity index (also known as quantitative Jaccard). In
231 most recent studies on the spatial distribution of phytoplankton, the common procedure is a
232 computation of Bray-Curtis dissimilarity matrix to define communities (Legendre and Legendre,
233 1998). However, Bray-Curtis generates a semi-metric matrix which is not as strong as the quantitative
234 Jaccard which generates a metric matrix for cluster analysis. Thus, the Jaccardized Czekanowski index
235 would be more suitable than Bray-Curtis for similarity studies (Schubert and Telcs, 2014). This
236 distance was computed per phytoplankton feature (*i.e.* abundance, red fluorescence) calculated from
237 the cytometric groups such as described in Bonato et al., (2015) in order to get the similarity between
238 pairs of samples. We processed the computation of an average similarity matrix between a matrix
239 based on abundance and a matrix based on red fluorescence. This method is more reliable than using
240 them separately because abundance and red fluorescence (proxy of chlorophyll content which in turn
241 is used as a proxy of biomass) are considered as the main features to discriminate the communities.
242 Each function was weighted between 0 and 1. Abundance accounted for 0.5 as well as red
243 fluorescence. We coupled the final similarity matrix with the Ward method (Ward, 1963) which
244 consist in aggregating at each step the two clusters with the minimum within-cluster inertia and detect
245 the homogeneity of the clusters. Then, the optimal classification cut level was obtained by selecting
246 the maximum average silhouette over the Cophenetic distances. These analyses were processed using

247 the packages “vegan”, “analogue” and “cluster” on R. The importance of environment and space
248 (defined as the Euclidean distance between a pair of latitude and longitude coordinates) for structuring
249 phytoplankton communities was studied among each community by processing a variation partitioning
250 (Borcard et al. 1992, Peres-Neto et al. 2006). In our model, the total variance is represented by four
251 fractions $[a + b + c + d]$ where $[a + b]$ represents the environmental fraction; $[b + c]$ represents the
252 space fraction; $[b]$ is the interaction between environment and space and $[d]$ the residual variance.
253 Space was redefined by the calculation of the principal coordinates of neighbour matrices (PCNM,
254 Borcard and Legendre, 2002) to define them as spatial descriptors of the relationship among sampling
255 units. We used the *pcnm* function from the “vegan” package design for R environment. Phytoplankton
256 communities were detrended using the Hellinger transformation which is appropriate for
257 compositional data by reducing the impact of rare events which are more susceptible to sampling error
258 (Legendre and Gallagher, 2001). In addition, transformation of the data will give the same weight to
259 rare or very abundant groups. Partitions were tested by ANOVA over 999 permutations. Finally, we
260 carried out a multivariate Mantel correlogram to investigate the relationship between geographical
261 distance extracted from the latitude-longitude coordinates and phytoplankton communities over the
262 water bodies. This analysis allowed the detection of the minimal distance at which the correlations
263 disappear.

264 3. Results

265 3.1 Hydrobiology

266 Each continuous-recorded physical variable as well as *in vivo* total fluorescence (μg equivalent of
267 chlorophyll *a* per L) showed a strong spatial structure. The highest salinity values were recorded in the
268 Western English Channel (35.5; WEC) and decreased moderately towards the East (35). In the Central
269 English Channel (CEC) salinity strongly decreased from 35 in offshore waters to 33 in the inner part
270 of the Bay of seine (BOS; Fig. 3A). Colder waters characterised the entrance of the WEC and were
271 surrounded by warmer waters both in the Celtic Seas as well as in mid WEC waters (Fig. 3B). Sharp
272 transitions were evidenced (of only a few kilometres) both at the West and East of the colder area.



273

274 Figure 3: Continuous recording of: **A.** Salinity, **B.** Temperature (°C) **C.** Turbidity (NTU) **D.**275 Chlorophyll *in vivo* Fluorescence ($\mu\text{g chl Eq L}^{-1}$).

276 The highest turbidity values were recorded in the CEC, both in offshore and coastal waters (Fig. 3C).
 277 A sharp increase in chlorophyll *in vivo* fluorescence was evidenced from the outer shelf to the WEC
 278 (values shifted from around 0.1 $\mu\text{g chl Eq L}^{-1}$ to 5.7 $\mu\text{g chl Eq L}^{-1}$). Then, fluorescence levels
 279 decreased rapidly eastward in WEC (from 5.7 $\mu\text{g chl Eq L}^{-1}$ to 1-1.5 $\mu\text{g chl Eq L}^{-1}$; Fig. 3D). Spearman
 280 ranks correlation were negative and significant with temperature ($\rho = -0.45$, $p < 0.001$) and turbidity
 281 ($\rho = -0.29$, $p < 0.001$) whereas Spearman rank correlation between fluorescence and salinity was
 282 positive and significant ($\rho = 0.31$, $p < 0.001$).

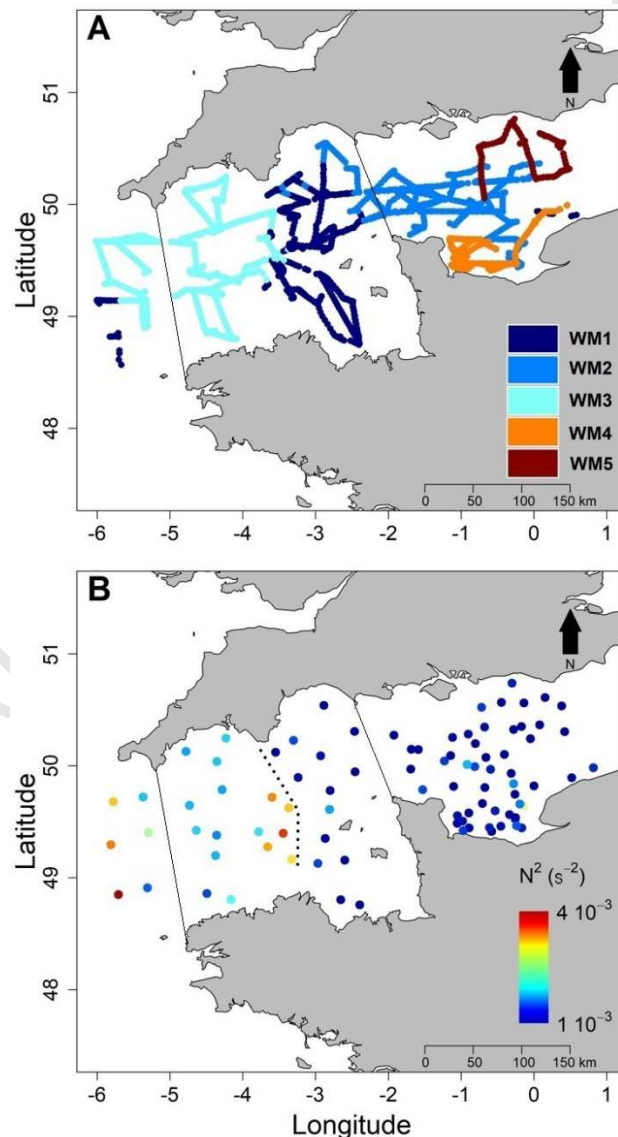
283 Applying hierarchical clustering on the similarity matrix revealed 5 water masses (WM) in the English
 284 Channel (Fig. 4A). Mapping these water masses revealed that Western and Central English Channel
 285 were structured in hydrological blocks. WM1 corresponded to the eastern part of the Western English
 286 Channel and Celtic Seas out of the Channel (Iroise and Irish Seas), whereas WM3 was located in
 287 between, in the centre of the WEC. WM2 was located in offshore waters mainly in the CEC. WM4
 288 was under the influence of the Bay of Seine and WM5 was considered as mainly corresponding to the
 289 English coastal and offshore waters of the CEC.

290 Table 1: Minimum and maximum values of temperature, salinity, turbidity and *in vivo* chlorophyll
 291 fluorescence (Chl Fluo) among the 5 water masses.

Water mass		Temperature ($^{\circ}\text{C}$)	Salinity	Turbidity (NTU)	Chl Fluo ($\mu\text{g chl Eq L}^{-1}$)
WM1	Min; max	[16.97; 18.84]	[34.04; 35.49]	[0.01; 3.35]	[0.31; 1.67]
	CV (%)	2.5	0.4	50	25
WM2	Min; max	[17.55; 18.95]	[33.17; 35.16]	[2.62; 4.87]	[0.11; 1.47]
	CV (%)	1.5	1.0	15	39
WM3	Min; max	[13.94; 18.12]	[35.16; 35.53]	[0.51; 1.31]	[0.49; 5.71]
	CV (%)	5.5	0.2	19	48
WM4	Min; max	[17.61; 18.31]	[33.11; 34.82]	[6.23; 14.28]	[0.57; 2.31]
	CV (%)	0.7	1.1	27	33
WM5	Min; max	[16.91; 17.93]	[33.78; 35.00]	[6.34; 18.73]	[0.59; 1.16]
	CV (%)	1.2	0.2	4.5	12

292
 293 The lowest temperature was recorded in the WM3 revealing also the strongest gradient ($\Delta T = 4.18^{\circ}\text{C}$,
 294 Fig.3B and table 1) whereas this water mass exhibited high stable salinity thus the lowest salinity
 295 gradient ($\Delta \text{SAL} = 0.37$, Fig.3A and table 1) among the water masses. The opposite pattern was
 296 observed in the WM1, WM2, WM4 and WM5, the difference of temperature was comprised between

297 0.70°C (WM4) and 1.87°C (WM1) with higher values than in WM3 whereas the salinity difference
 298 was comprised between 1.22 (WM5) and 1.99 (WM2) with lower values than in the WM3. Turbidity
 299 was also lower in WM3 than in any other WM and showed a small difference ($\Delta\text{TURB} = 0.8$ NTU).
 300 The highest range of turbidity values were found in the WM4 and WM5 (respectively $\Delta\text{TURB} = 8.05$
 301 NTU and $\Delta\text{TURB} = 12.39$ NTU), both WM under the influence of the Solent (UK) and Seine (France)
 302 estuaries. In WM3, *in vivo* chlorophyll fluorescence (Chl Fluo) was higher than in any other water
 303 mass and showed the highest variability ($\Delta\text{Chl Fluo} = 5.22 \mu\text{g chl Eq L}^{-1}$).



304

305 Figure 4: **A.** Identification of water masses based on results from the Euclidean distance matrix on
 306 temperature, salinity, turbidity and *in vivo* chlorophyll fluorescence. **B.** Stratification, value of N^2 , as

307 derived from CTD casts. The dashed line distinguishes homogeneous water masses from
308 heterogeneous water masses and marks the front.

309

310 On the West of the main frontal structure (WEC, Fig. 4B), corresponding to WM3, N^2 values were
311 higher and displayed more heterogeneous waters than in the East side (CEC and BOS), where the
312 values of N^2 were lower and displayed homogeneous waters. In the WEC (WM3), N^2 values reached
313 up to 10^{-3} s^{-2} whereas in the CEC and the BOS (WM2, WM4 and WM5), the order of magnitude of N^2
314 values was between 10^{-4} and 10^{-5} s^{-2} (Fig. 4B). In the Celtic seas, the N^2 was recorded between 3.5 and
315 $4.5 \cdot 10^{-3} \text{ s}^{-2}$ decreasing sharply eastward with the shift of temperature to reach $1.5 \cdot 10^{-3} \text{ s}^{-2}$ in the WEC.
316 They define the outer thermal front as well as the western limit between WM1 and WM3. Then a
317 second change occurred between the WEC and the CEC. The values of the N^2 in WM3 of up to $4.0 \cdot 10^{-3}$
318 s^{-2} shifted to $10^{-4} / 10^{-5} \text{ s}^{-2}$ the CEC (WM2, WM4) and the BOS (WM5) defining the inner thermal
319 front.

320 **3.2 Phytoplankton abundance, fluorescence and spatial distribution.**

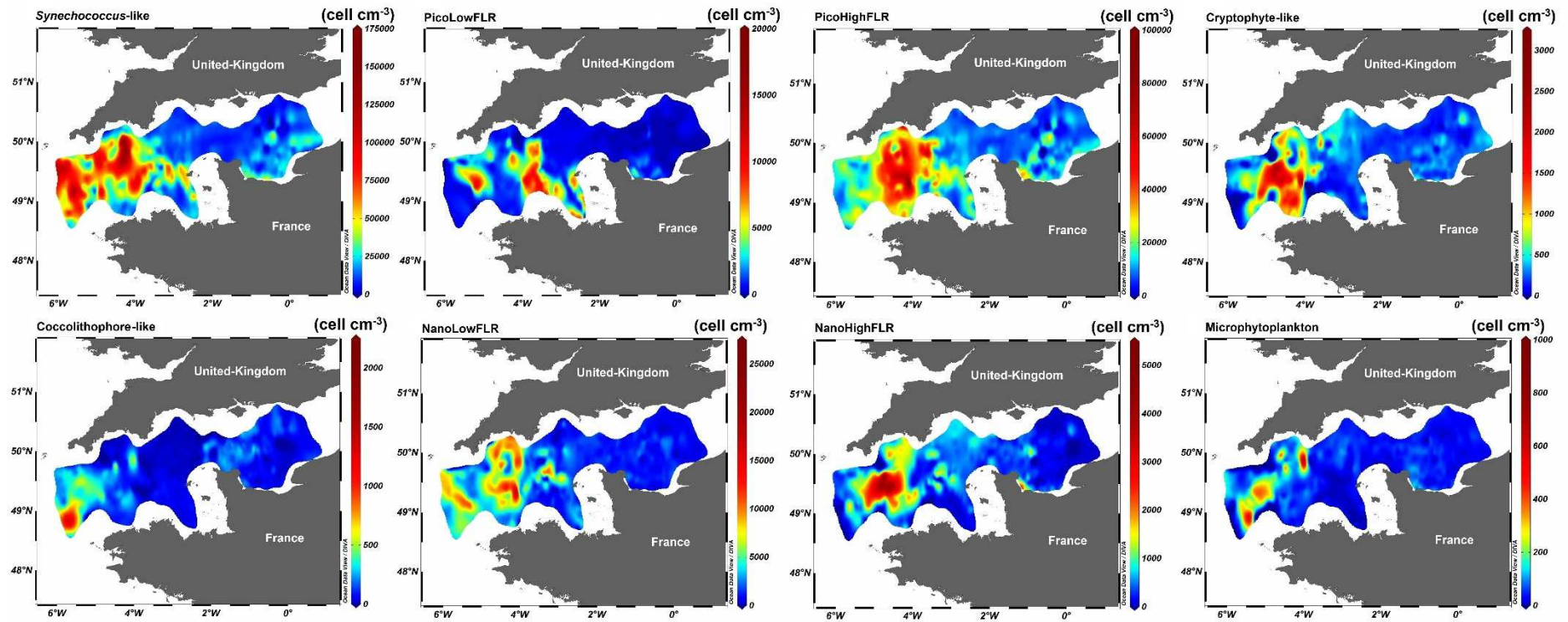
321 Picoeukaryotes (PicoLowFLR and PicoHighFLR) and *Synechococcus*-like cells dominated the
322 phytoplankton abundance. They were structured along a decreasing West-East longitudinal gradient
323 but showing an important heterogeneity in spatial distribution (Fig. 5). High abundance was recorded
324 in the Western English Channel (mostly in WM3) whereas low values were recorded in the Central
325 English Channel and, for Picoeukaryotes, at the western entrance of the English Channel (Celtic Seas,
326 Fig. 5 and 6). However, the abundance of *Synechococcus*-like cells was high out of the Channel and in
327 the WEC, and low in the CEC (Fig. 5A). PicoLowFLR abundance exhibited patches reaching more
328 than $1 \times 10^4 \text{ cell mL}^{-1}$ in the WEC (5% of the highest abundance were representing 950 km^2) and close
329 to the Channel isles (Fig. 5B). PicoHighFLR (Fig. 5C) and Cryptophyte-like cells (Fig. 5D) showed
330 the same patterns: low abundance out of the English Channel, sharp increase and high abundance in
331 the WEC (both coastal and offshore waters, WM3), then a sharp decrease and low abundance in the
332 eastern WEC and CEC. Coccolithophore-like cells (Fig. 5E) exhibited high abundance out of the

333 Channel (western WM1), while the abundance remained low elsewhere. NanoLowFLR (Fig. 5F)
334 showed several patches of high abundance (5% of the highest abundance represented 1000 km²)
335 between the limits of WM3 (out of the Channel and in the WEC). In the CEC and BOS, the abundance
336 was low. NanoHighFLR high abundance was also detected in WM3, forming a large patch in offshore
337 waters of the WEC (Fig. 5G), decreasing westward and eastward, showing an increase in a restricted
338 area in the Bay of Seine. Microphytoplankton abundance (Fig. 5H) was low out of the English
339 Channel. Then, patches of high abundance were observed in western WM3, in offshore waters of the
340 WEC. In the CEC and BOS, the abundance was low.

341 The abundance of each group was compared with respect to the distance of the inner WEC thermal
342 tidal front used as an arbitrary geographical reference (Ushant front, Fig. 6). Samples located to the
343 West of the front were represented by a negative distance whereas samples located to the East of the
344 front were represented by a positive distance. A global view revealed that abundance increased as the
345 sample got collected closer to the Ushant frontal area (Fig. 6). This was the case for PicoHighFLR
346 (Fig. 6.C), Cryptophyte-like cells (Fig. 6.E), and NanoLowFLR (Fig. 6.F). On the other hand,
347 NanoHighFLR (Fig. 6.G.) and Microphytoplankton groups (Fig. 6.H.) showed maximum abundance
348 slightly offset (westward) of the front (microphytoplankton also showing high values all along the
349 front). For these groups (PicoHighFLR, Cryptophyte-like cells, NanoLowFLR, NanoHighFLR and
350 Microphytoplankton), the highest levels of abundance were recorded in WM3 which is the most stable
351 water mass observed here. PicoLowFLR (Fig. 6.B), *Synechococcus*-like cells and Coccolithophore-
352 like cells showed a different pattern. The first two groups exhibited high abundance along and across
353 the front in the Western English Channel and in the Celtic Seas (Fig. 6.A) whereas Coccolithophore-
354 like cells showed highest abundance only in shelf waters at the western entrance of English Channel
355 (Fig. 6.D) where waters remained warm and stable (outer front of the WEC). At the East of the inner
356 front, the abundance decreased slowly to reach low values at 100 km from the main frontal system
357 (Fig. 6). At 200 km from the front, a second increase of abundance was observed (Fig. 6) for some
358 groups. A *Synechococcus*-like cells (Fig. 6.A.), PicoLowFLR (Fig. 6.B), PicoHighFLR (Fig. 6.C),
359 NanoHighFLR (Fig. 6.G) and, to a lesser extent, Microphytophytoplankton (Fig. 6.H) and

360 Coccolithophore-like cells (Fig. 6.D) showed high values compared to the remaining CEC. However,
361 this second peak was 2 to 3 times lower than the one observed close to the main front and could be
362 related to the Seine river plume.

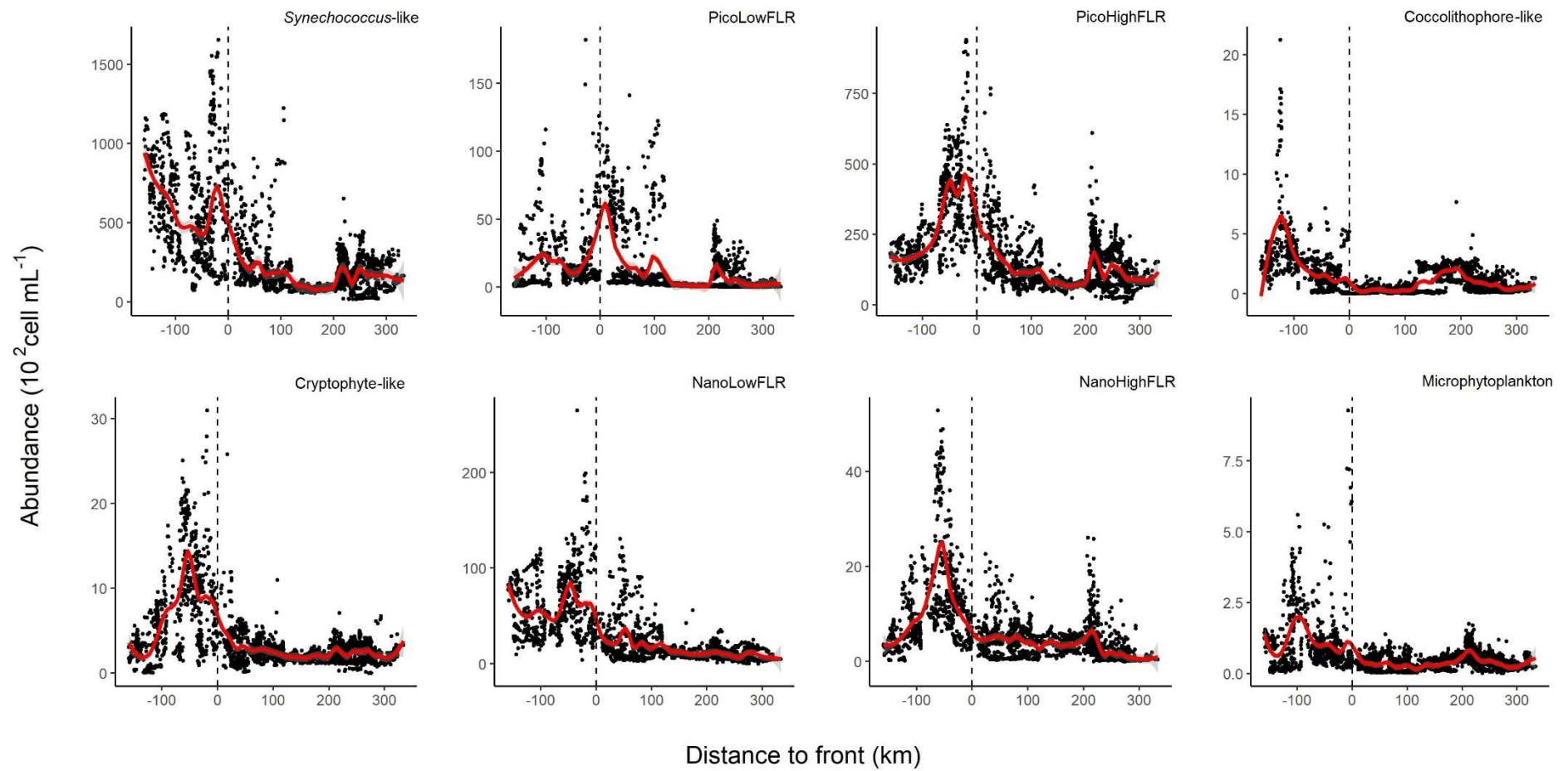
Journal Pre-proof



363

364 Figure 5: Spatio-temporal distribution of the abundance of the eight phytoplankton groups characterised by the PSFCM.

365



366

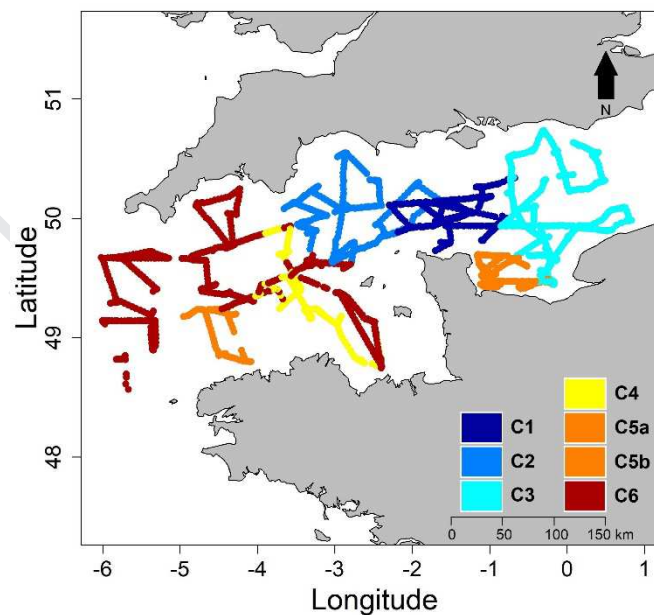
367

368 Figure 6: Distribution of the abundance in relation to the distance to the Ushant front (km) for the eight phytoplankton groups characterised by the CytoSense.
369 The dashed line represents the position of the inner thermal front. Negative distance represents samples at the West of the front. Positive distance represents
370 samples at the East of the front.

Journal Pre-proof

371 3.3 Phytoplankton communities structure analysis.

372 Phytoplankton communities were discriminated after the computation of a hierarchical classification
 373 of the quantitative Jaccard index on abundance and red fluorescence (Fig. 7). The Analysis of
 374 Similarity (ANOSIM) provided evidence of a spatial clustering of 6 communities ($R = 0.50$, $P =$
 375 0.001). However, due to discontinuity between the community C5, we split C5 in C5a and C5b for the
 376 investigation of the spatial scale analysis. C1 and C2 were characterised in offshore waters between
 377 WEC and CEC (mainly eastern offshore part of WM1 and offshore WM2. C3 was found in the Central
 378 English Channel and characterised also the Eastern part of the Bay of Seine (BOS), mainly WM2 and
 379 WM5. C4 was located by the inner thermal front (Fig. 4B). C5 community was found in the Western
 380 part of the BOS (WM4; C5a) and also in the French part of the WEC (WM3; C5b). C6 corresponded
 381 to most of the WEC offshore waters (WM3) including external Channel stations (western part of
 382 WM1).



383

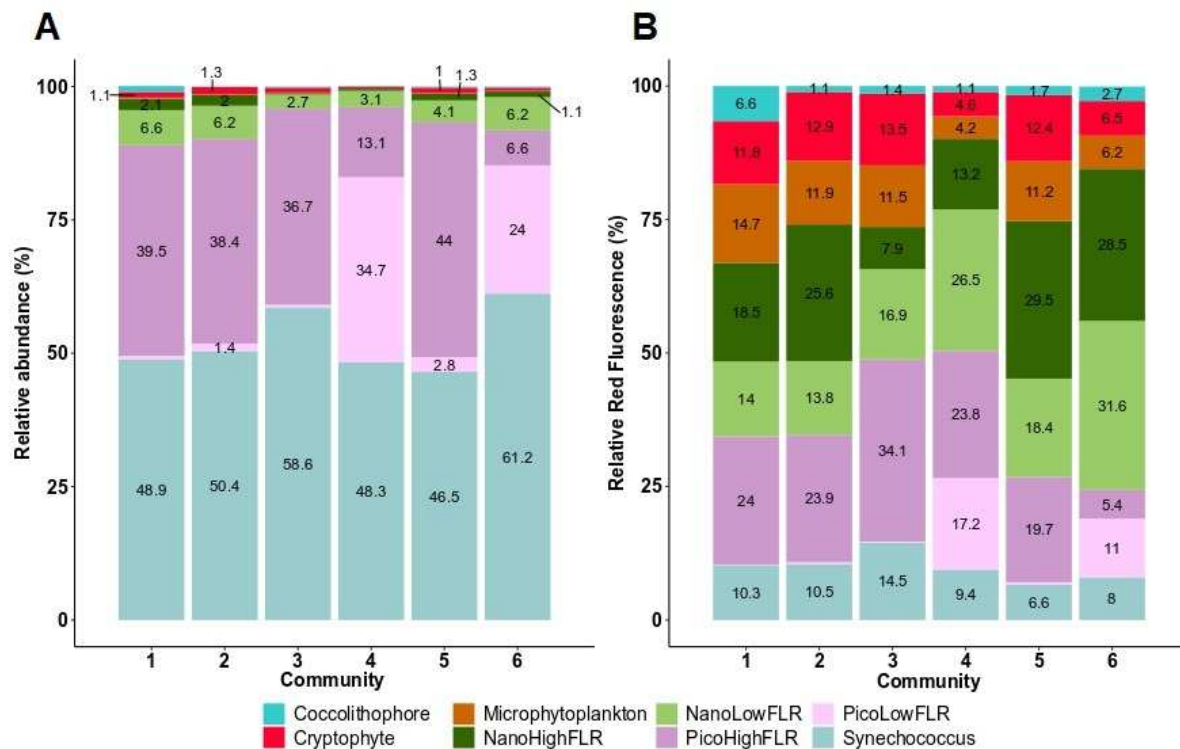
384 Figure 7: Phytoplankton communities based on the results of the fusion between Jaccard similarity
 385 matrice on the abundance and red fluorescence.

386 Heterogeneity was supported by the values of the coefficient of variance (CV) calculated for each
 387 group, in addition, to minimum, maximum of abundance and total red fluorescence (further details in

388 supplementary table A.1). In terms of abundance (Fig. 8), phytoplankton communities were all
389 dominated by the *Synechococcus*-like group (47% in C5 to 61% in C6 to the total abundance).
390 Picoeukaryotes (*i.e.* PicoLowFLR and PicoHighFLR) groups represented the second most important
391 groups (Fig. 8). However, in C1, C2, C3 and C5, the PicoLowFLR (36% in C3 to 43% in C5)
392 dominated over the PicoHighFLR (1% in C1, C2 and C3 to 3% in C5) whereas in C4 and C6, the
393 PicoHighFLR (24% and 34% respectively in C4 and C6) dominated over the PicoLowFLR (7% and
394 13% respectively in C6 and C4). On the other hand, the total abundance of nanoeukaryotes was always
395 low (at most they represented 11% of the total abundance for C1). The most abundant nanoeukaryotes
396 group was NanoLowFLR (3% in C3 and C4 to 7% in C1). In C2, the Cryptophyte-like cells total
397 abundance was the double than in any other assemblages. The most important contribution of the
398 Coccolithophore-like cells was found in C1 (1%) whereas in the other communities they accounted for
399 less than 1%. Finally, the total abundance of the microphytoplankton in every community was below
400 1%.

401 Although small photoautotrophs significantly dominated abundance (Fig. 8) in both WEC and CEC
402 during the cruise, the contribution of nanoeukaryotes and microphytoplankton to total red
403 fluorescence, which is an estimation of chlorophyll *a* fluorescence (Haraguchi et al., 2017), was
404 important (supplementary table A.1, Fig. 8). The relative contribution of the Coccolithophore-like
405 cells to the total red fluorescence was almost seven times higher in C1 than in any other community.
406 On the other hand, nearly half of the total red fluorescence in C3 and C4 was attributed to
407 *Synechococcus*-like and picoeukaryotes groups (C3: 49% and C4: 50%). This was higher than in the
408 other communities (range between 25% in C6 to 34% in C1 and C2). In C1, C2, C3 and C5,
409 Cryptophyte-like cells total red fluorescence represented the double (12-13%) of what they
410 represented in C4 and C6 (respectively 5% and 6%). In C3, C4 and C6, NanoLowFLR contribution to
411 the total red fluorescence (respectively C3: 17%; C4: 27% and C6: 32%) was higher than the
412 contribution of the NanoHighFLR (C3: 8%; C4: 13% and C6: 29%). We noticed the opposite pattern
413 in C1, C2 and C5. Despite the low abundance of the microphytoplankton group, the contribution to
414 total red fluorescence of this group was comprised between 4% (C4) and 15% (C1).

415



416

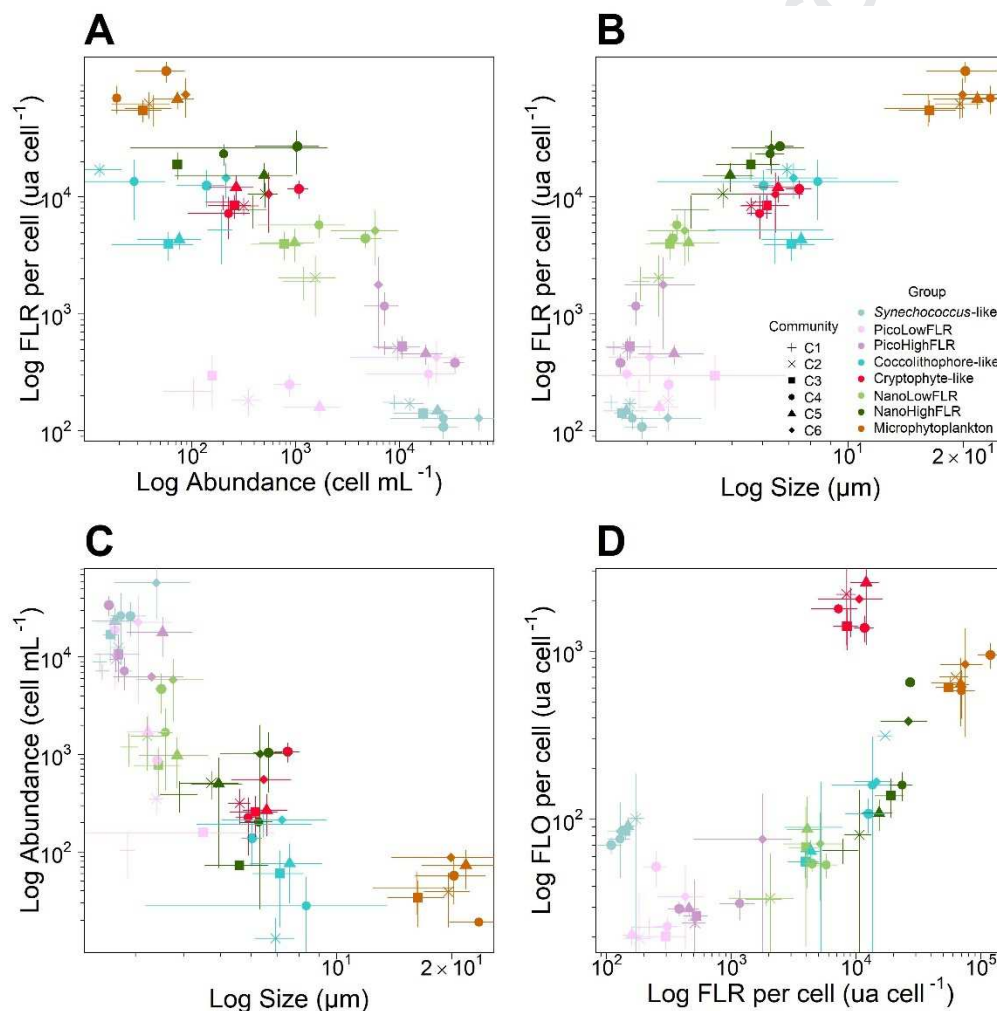
417 Figure 8: Relative contribution of phytoplankton, A. abundance and B. total red fluorescence, within
 418 each community. Only the percentage above 1% are displayed.

419 Although we observed an heterogeneity in total red fluorescence per cluster, the CytoSense provided
 420 us with information on single-cell level features (Fig. 9). Therefore, working at the individual level led
 421 us to study the population variability considering a cytometric-derived trait. Here, we first focused on
 422 the red fluorescence per cell and then on the cell-size. Different spatial patterns of red fluorescence per
 423 cell and cell size were observed, per group, among the communities. *Synechococcus*-like red
 424 fluorescence per cell remained unchanged in all the communities despite changes in cell size and
 425 abundance (Fig. 9 A and B). Cell size was significantly different between all the communities
 426 identified ($p < 0.01$). Both picoeukaryote groups (*i.e.* PicoLowFLR and PicoHighFLR) exhibited the
 427 most important red fluorescence per cell in C4 and C6 than in the other communities ($p < 0.05$). For the
 428 PicoLowFLR, the community comparison showed a large range of abundance within an order of
 429 magnitude of $10^2 \text{ cell mL}^{-1}$ whereas red fluorescence level remained between 200 and 400 a.u. cell^{-1}
 430 (Fig. 9A). An increase in the red fluorescence per cell was observed with an increase of the cell size

431 (Fig. 9B). On the contrary, for the PicoHighFLR, high red fluorescence levels were consistent with
432 low abundance (Fig. 9A) and different relation between red fluorescence and cell size were observed
433 (Fig. 9B). Small cell with high red fluorescence levels were found in C4 and C6. Small cell with low
434 red fluorescence were found in C1, C2 and C4 and large cell with some level of red fluorescence were
435 found in C3. Concerning Cryptophyte-like cells and Microphytoplankton groups, the highest red
436 fluorescence values per cell were found in C5 and C6 and were significant ($p < 0.05$). In these
437 communities, the Cryptophyte-like cells exhibited also the highest abundance (Fig. 9A and B) and
438 their cell size was significantly larger in C4, C5 and C6 than in C1, C2 and C3 ($p < 0.05$).
439 Coccolithophore-like cells showed higher red fluorescence per cell in C2, C4 and C6 than in C1, C3
440 and C5. Moreover, the highest values of red fluorescence per cell were observed for NanoLowFLR
441 and NanoHighFLR in C4, C5 and C6. Finally, larger cell size was recorded in C4, C5 and C6 than in
442 C1, C2 and C3 for PicoLowFLR, Coccolithophore-like cells, NanoLowFLR and NanoHighFLR, but
443 no pairwise assemblage was significantly different. The log-log relation between red fluorescence and
444 orange fluorescence, per cell, showed an increase in fluorescence emission with the cell size (Fig. 9B).
445 In addition, there was an increase in the red and orange fluorescence emission as the cell size increases
446 (Fig. 9D) despite the standard deviation showed large variation for the orange fluorescence.

447 For red fluorescence, three orders of magnitude were recorded from the smallest (*Synechococcus*-like
448 cells) to microphytoplankton cell size. *Synechococcus*-like and Cryptophyte-like cells could be
449 characterized by a higher orange over red ratio from the other groups. However, not all groups
450 subscribed to this relation. Indeed, the figure 10B showed that some groups exhibited a change in size
451 but not in red fluorescence per cell (range of the standard deviations). This occur in specific
452 communities or in each community. For example, PicoHighFLR exhibited a large range of cell size
453 and red fluorescence in C6 and C1 whereas the size and the red fluorescence were fluctuating
454 irrespective to each other in the rest of the communities. Such patterns were also observed for the
455 Coccolithophore-like cells. This relation would mean that in some case the red fluorescence per cell is
456 independent of the size of the cells. As chlorophyll *a* fluorescence reflects the endogenous
457 concentration of this pigment, the relation between red fluorescence per cell and cell size may result

458 different intracellular pigment composition (Álvarez et al., 2017). On the other hand, the other groups
 459 (*i.e.* *Synechococcus*-like cells, PicoLowFLR, nanoeukaryotes, microphytoplankton and Cryptophyte-
 460 like cells) tended to show a balance between the size and the red fluorescence, the larger a cell was,
 461 the more red fluorescence it would emit. Finally, the range of the standard deviation in red and/or
 462 orange fluorescence emission showed that the emission of red fluorescence per cell within
 463 PicoLowFLR, PicoHighFLR, NanoLowFLR, NanoHighFLR, Cryptophyte-like cells and
 464 Coccolithophore-like cells groups were not proportional to the emission of orange fluorescence per
 465 cell. On the contrary, the emission of red fluorescence per cell was proportional to the emission of
 466 orange fluorescence per cell concerning *Synechococcus*-like cells and Microphytoplankton (Fig. 9D).



467

468 Figure 9: Patterns in size structure and fluorescence of phytoplankton groups amongst different
 469 communities defined in the English Channel. A. Log-log relationship between phytoplankton

470 abundance and the red fluorescence per cell, per group and per community, B. Log-log relationship of
471 the red fluorescence per cell (FLR) against the phytoplankton size scaling per group and per
472 community, C. Log-log relationship between phytoplankton cell size and abundance per group and per
473 community, D. Log-log relationship of the orange fluorescence per cell (FLO) against the red
474 fluorescence per cell (FLR) per phytoplankton group and per community.

475 **3.4 Variance partitioning**

476 Results of the variance partitioning (pure spatial, pure environmental, interaction between environment
477 and space and unexplained variance) of the whole phytoplankton community and of each of the six
478 assemblages were summarized in table 2. Such analysis revealed that spatial (PCNM spatial
479 descriptors) and environmental variables (temperature, salinity and turbidity) accounted for 65% of the
480 total variance on the whole cruise. The 35% of the residual variance (*i.e.* unexplained variance) were
481 explained by other factors than environmental variables and space (*e.g.* biological processes such as
482 grazing, infection without interaction with the environmental data; Table 2). The spatial descriptors
483 (based on the spatial coordinates of sampling points) were more important than the environmental
484 variables (<5% for all the groups) in structuring the abundance and total red fluorescence of each
485 group. The spatial descriptors ranged between 24% (Coccolithophore-like cells) and 34%-36% (all the
486 other groups). The results were provided in the supplementary table A.2. Focusing on the
487 communities, the spatial variation of the assemblages was higher than the environmental variation
488 within C1, C2, C3, C5 and C6. In community C4, the environmental variation accounted for 45% and
489 was similar to the spatial variation which accounted for 43%. Then, the spatially structured
490 environment (*i.e.* interaction) accounted between 13% (C1) and 46% (C6) of the total variation.
491 Finally, considering the six communities identified (C5a and C5b are merged), both spatial and
492 environmental variables accounted for a significant amount of variation except for the effect of the
493 interaction between environment and space in C1. The sum of pure spatial, pure environmental
494 variables and their interaction explained from 40% (C1) to 74% (C6) of the total variation in the
495 communities. Therefore, the percentage of unexplained variation in the phytoplankton assemblages
496 was comprised between 26% (C6) and 60% (C1).

497

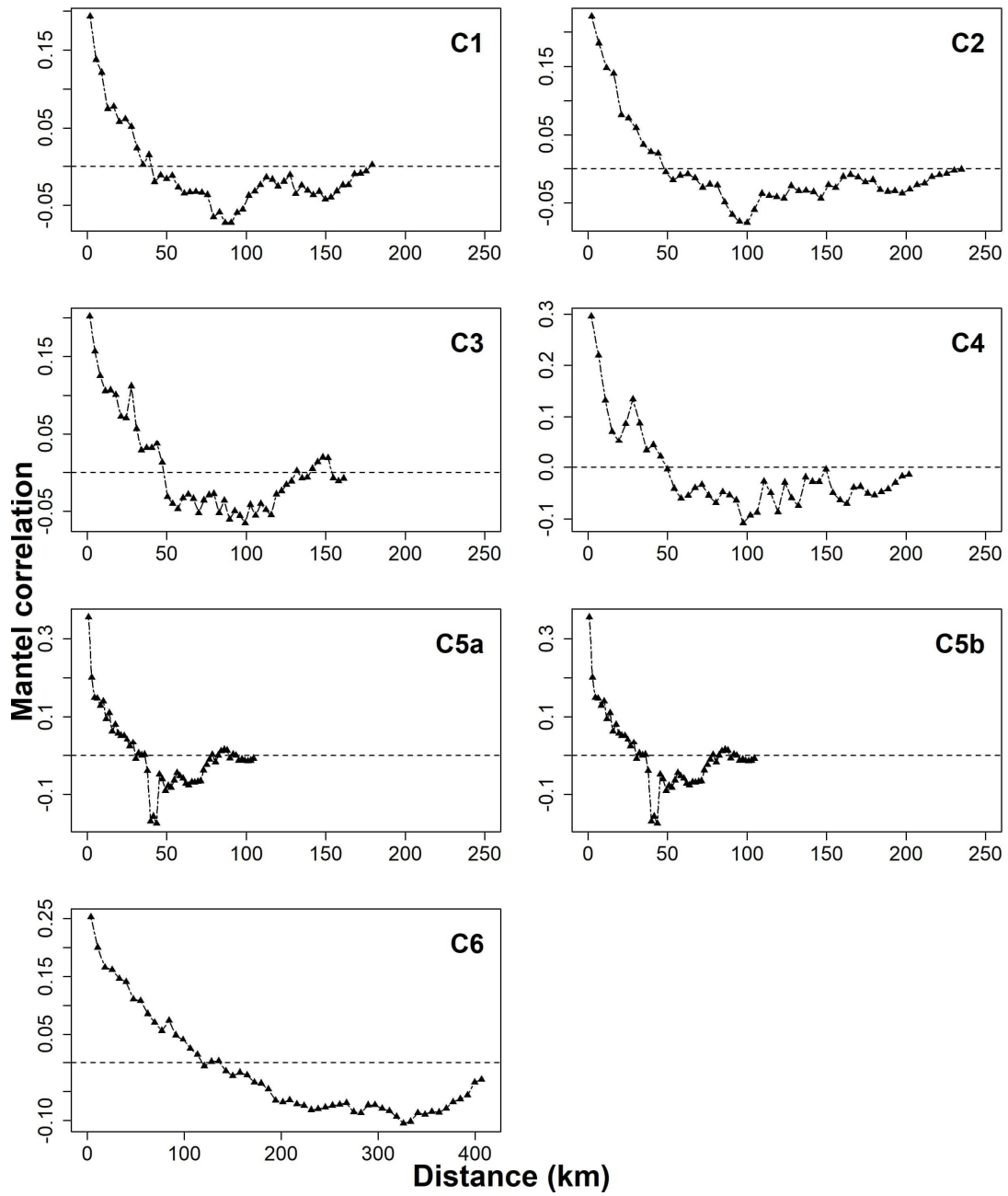
498 Table 2: Variation partitioning of phytoplankton community (Environment including temperature,
 499 salinity and turbidity; space including abiotic interactions, physical processes and unexplained
 500 environment).

	Environment		Space		Interaction		Residual
	R ² Adj.	p-value	R ² Adj.	p-value	R ² Adj.	p-value	
All	0.26	0.001	0.65	0.001	0.26	0.001	0.35
C1	0.15	0.001	0.25	0.001	0.13	0.06	0.60
C2	0.19	0.001	0.51	0.001	0.16	0.001	0.47
C3	0.59	0.001	0.60	0.001	0.43	0.001	0.34
C4	0.45	0.001	0.43	0.001	0.36	0.001	0.49
C5	0.35	0.001	0.44	0.001	0.27	0.001	0.48
C6	0.50	0.001	0.70	0.001	0.46	0.001	0.26

501

502 3.5 Scale of variability of phytoplankton communities

503 The multivariate Mantel correlogram based on the abundance and the average total red fluorescence
 504 per cluster revealed phytoplankton communities' spatial pattern by computing the geographical
 505 distance between pairs of sites in each community (Fig. 10). The Mantel correlogram indicated the
 506 highest autocorrelation at nearer distances, with a decrease and always reaching negative values at
 507 farther distances (but not always at the same distance). Because C5 community was not spatially
 508 continuous, C5 community was split into C5a (Eastern Bay of Seine) and C5b (South-Western of the
 509 WEC) sub-groups. The highest autocorrelation was found in C4 and C5b ($r=0.34$ and $r=0.40$,
 510 respectively). Phytoplankton assemblages showed a positive spatial autocorrelation between 20 km
 511 (C5a) and 110 km (C6, Fig. 11). This meant that phytoplankton composition became more different
 512 when the autocorrelation reached null or negative values. The definition of the spatial scale resulted in
 513 the combination of high correlation for the nearer distances and the quick decrease of the correlation
 514 when the distance increased. Here, the results suggested a high spatial structure at sub-mesoscale (<10
 515 km) up to 110 km. This analysis confirmed the results of the partitioning variance analysis which
 516 mentioned that space had a great influence in structuring the assemblages.



517

518 Figure 10: Mantel Correlogram of pairwise similarity in phytoplankton communities (Jaccardized
519 Czekanowski similarity based on the abundance and average total red fluorescence per cluster) against
520 geographical distance (Euclidean distance).

521

522 4. Discussion

523 4.1 Water masses

524 Despite the English Channel is a rather well-studied area, only few surveys attempted to characterise
525 the spatiotemporal distribution of physicochemical parameters in the CEC and WEC (Bentley et al.,
526 1999; Charria et al., 2016; Garcia-Soto and Pingree, 2009; Napoléon et al., 2014, 2012). Most studies
527 benefited of long-term coastal monitoring or transect of ships-of-opportunity through a year. In the
528 present study, the focus was put in the whole Western and Central English Channel gridded at a
529 specific period of a year. Although the sampling strategies differed, our results showed similar
530 hydrological areas than previous studies. The water circulation from West to East in the English
531 Channel explained the longitudinal gradient observed during our study especially for the slow salinity
532 decrease (Salomon and Breton, 1993). In addition to this circulation, the vertical stability induced
533 during summer, contributed to the longitudinal gradient of temperature. Along the English coast of the
534 Central English Channel, the high values of turbidity were congruent with continuous run-off from the
535 Solent and were entertained in the gyre of the Southern part of the Isle of Wight (Ménèsquen and
536 Gohin, 2006). During the CAMANOC cruise, strong horizontal gradients of temperature, salinity and
537 turbidity revealed five distinct water masses. The temperature gradient revealed tidal mixing fronts
538 where a strong stratification occurred (Simpson and Nunes, 1981). The stratification of the Ushant
539 frontal area (Garcia-Soto and Pingree, 2009; Pingree, 1980; Pingree et al., 1975; Pingree and Griffiths,
540 1978) separated 2 water masses (WM). WM3 corresponded to Western English Channel (WEC)
541 waters displaying mixed water column, lower temperature and higher salinity than the rest of the
542 waters of the outer Channel (shelf front) and the eastern WEC. WM3 was surrounded by stratified
543 waters. The western boundary corresponded to an external front separating warm and stratified waters
544 (Celtic Seas shelf waters) from mixed and cold waters (WM3). At the east, an internal front separated
545 cold and mixed waters (WM3) from warm and well-mixed waters (WM1). The temperature pattern
546 observed in the offshore waters was not consistent with observation in 2011 (Marrec et al., 2013;
547 Napoléon et al., 2013) but was congruent with negative anomaly observed in 2012 in the northern part
548 of the WEC (Marrec et al., 2014). We explained that by a combination of a relatively higher stability
549 of water in WM3 (low tidal stream) than in the CEC (high tidal stream) and the lower temperature
550 which are supported by air-sea heat fluxes shifting from positive to negative balance during the
551 summer-autumn transition. Thus, the upper mixed layer deepens and water cools down (Hoch and

552 Garreau, 1998). WM1 was characterized by high stable temperature and salinity (Fig. 4B). It might
553 have corresponded to the external front separating the WEC and the Celtic Seas in the Western border
554 and the internal front between the WEC and the CEC in the Eastern border. A latitudinal salinity
555 gradient revealed a salinity front separating WM4 found in the Bay of Seine (BOS) from the CEC
556 waters (WM2). The turbidity gradient separated the offshore waters of the CEC from English coastal
557 waters of Central English Channel (WM5). The low values of N^2 in WM4 (BOS) resulted from
558 permanently mixed waters even under the influence of the run-off of the Seine River (Bay of Seine;
559 French coast) whereas WM5 might have been under the remote influence of the Solent (English
560 Coast), leading to a slight dilution of coastal waters (compared to lower salinities recorded in the Bay
561 of Seine). WM2 could result in intermittently stratified waters (Van Leeuwen et al., 2015) in the
562 continuity of WEC stratified waters.

563 **4.2 Phytoplankton communities**

564 Several studies attempted to numerate phytoplankton assemblages in the whole area of the WEC and
565 CEC but none of them with high spatial (Garcia-Soto and Pingree, 2009; Napoléon et al., 2014, 2013,
566 2012) expanded gridding of data or on high temporal resolution (Edwards et al., 2001). Furthermore,
567 in this area, while previous studies focused only on species of the large size fraction of the
568 phytoplankton (*i.e.* microphytoplankton; Napoléon et al., 2014, 2012; Smyth et al., 2010; Tarran and
569 Bruun, 2015; Widdicombe et al., 2010), we were able to detect the whole size-range of phytoplankton
570 from picophytoplankton (1 μm) to large microphytoplankton (several millimeters length) in a single
571 analysis. Even though we did not reach a taxonomical resolution, it was possible to address the fine
572 structure of phytoplankton functional groups, as well as some of their traits, during the summer-
573 autumn transition.

574 In this study, we used the CytoSense parameters derived from the optical features and signatures as
575 cytometric-derived traits at the individual and populational level (Violle et al., 2007) while several
576 studies were applying the same technique and approach in different aquatic ecosystems focusing only
577 one level (Fragoso et al., 2019; Malkassian et al., 2011; Pomati et al., 2011; Pomati and Nizzetto,
578 2013). The four selected traits (abundance per group, orange and red fluorescence per cell and cell

579 size) showed a spatial heterogeneity for each group, between the communities (Litchman et al., 2010).
580 The cell size was independent of cell's physiology per group between our communities (larger cells
581 and higher average red fluorescence per cell in the community of the WEC, C4 and C6 than in the
582 communities of CEC and BOS, C1, C2, C3 and C5). This result suggests specific responses of the
583 species and/or groups. Indeed, in order to explain the spatial heterogeneity of the traits, we propose
584 three hypothesis: (i) the selection of the optimal traits under biological pressures such as grazing
585 (Litchman et al., 2009); (ii) the plasticity and genetic adaptation of the traits derived from the gene
586 expression in response to environmental variations (Litchman et al., 2010) and; (iii) in the case of the
587 automated "pulse shape" flow cytometry, a group can pool several species with similar optical
588 properties (Thyssen et al., 2008a). Here, as grazers were not recorded continuously, we decided not to
589 discuss about this hypothesis but would rather investigate the two others.

590 First, we suggest that the main drivers of the spatial variations are the temperature and the vertical
591 stability of water masses. The results showed that PicoLowFLR group, Cryptophyte-like cells,
592 nanoeukaryotes and microphytoplankton of the communities characterizing stratified and warm waters
593 (C4) and mixed and cold waters (C6) exhibited the largest average cells size and the highest red and
594 orange fluorescence per cell. Because the optimum for growth range of both nanoeukaryotes and
595 microphytoplankton is relatively low, the colder temperatures measured in WM3, characterized mainly
596 by C6, might have contributed to enhance their metabolism, hence, their size (Marañón, 2015). On the
597 contrary, despite small phytoplankton (picophytoplankton) are dominant everywhere at this period,
598 their growth is facilitated in water masses exhibiting high temperature values (C1 to C5, all WM
599 except WM3). Indeed, their temperature optimum for growth range is higher than nanophytoplankton
600 and microphytoplankton optimum growth range and should favor them in those conditions. Thus, in
601 water masses exhibiting cold water, we expect a dominance of larger cell size whereas in warmer
602 waters a dominance of the smaller cell size within a group. Although, nutrient and grazing rate were
603 not available at the same spatiotemporal resolution as the biological data, we are aware that both play
604 a role on cell size as well as their physiology. In the first case, the growth of small cells (*i.e.*
605 *Synechococcus*-like cells and picoeukaryotes) is favored against large cells (*i.e.* microphytoplankton)
606 under low nutrient condition (usually from the end of the spring bloom to fall). Then, biological

607 interactions (grazing, parasitism) are usually to impact cell size (Bergquist et al., 1985; Marañón,
608 2015) and physiology (Litchman, 2007; Litchman et al., 2010; Litchman and Klausmeier, 2008).
609 Finally, size overestimation of *Synechococcus*-like cells and picoeukaryote (Fig. 9) results of technical
610 drawbacks of flow cytometry. It is attributed to the halo effect of the laser which increased as particle
611 were increasingly smaller than the width of the laser beam (*i.e.* 5 μ m).

612 The heterogeneity of environmental conditions within a water mass affect the expression of the traits
613 within each group. For example, the Coccolithophorids are known to prefer warm and stable waters
614 (WM1) for their growth. Here, the PSFCM detected high total abundance of this group in the Celtic
615 Seas shelf, out of the English Channel (WM1, Fig. 5 and 6) which are dominated in this range of
616 abundance by *Emilinia huxleyi* (Garcia-soto et al., 1995). On the contrary, microphytoplankton
617 (including some diatoms and dinoflagellates) are known to grow and exhibit higher size in cold
618 waters, turbulent system, rich in nutrient. This explanation is also true for the nanoeukaryotes (*i.e.*
619 NanoLowFLR and NanoHighFLR). This is congruent with the WM3 and WM4 being influenced by
620 the Seine river (C5) and both by the Atlantic Ocean waters and the Seine River (C3). They both
621 contribute to provide nutrients. In addition, the low vertical water stability observed in the coastal
622 communities (along the French coast of Brittany, Bay of Seine) could increase small-scale turbulence
623 which might be positive for some groups (microphytoplankton, Cryptophytes-like, nanoeukaryotes) by
624 increasing nutrient transport (Karp-Boss et al., 1996).

625 On the other hand, all the groups exhibited different levels of red and orange fluorescence per cell
626 between the communities, except *Synechococcus*-like cells which showed the same levels across the
627 communities (Fig. 9A, B and D). The fluorescence emission given by each group is dependent on the
628 physiological states of the cells. The quantum yield of the chlorophyll *a* fluorescence (*i.e.* red
629 fluorescence of the PSFCM) and phycobilin and phycoerythrin (*i.e.* orange fluorescence of the
630 PSFCM) is also dependent to the life cycle of the cells leading to high fluorescence for young and
631 efficient cells whereas lysis is decreasing the fluorescence emission. Another point was linked to the
632 atmospheric conditions during the cruise. At the beginning of the cruise (corresponding mainly to
633 communities C6, C5 and C4 in WEC waters), the weather was sunny and without wind, some groups
634 (picoeukaryotes, nanoeukaryotes and microphytoplankton) showed high variability in orange

635 fluorescence per cell within a single community. The strong light intensity and the high stability might
636 have resulted in the synthesis of photoprotective pigments. However, the change of weather after half
637 of the cruise (while investigating WM3 and C1) might have enhanced the vertical mixing. Therefore,
638 the position of phytoplankton cells of the groups is permanently engendered by the mixing of the
639 water column which do not the induce production of photoprotective pigments.

640 Finally, the last case concerns the lack of taxonomical resolution of the automated “pulse shape-
641 recording” flow cytometer. Indeed, our number of groups was limited. By sharing similar optical
642 properties, several species are attributed to a same cluster. In WEC waters, flow cytometry surveys
643 showed that picophytoplankton is usually composed of Prasinophyceae and usually dominated by
644 *Ostreococcus sp.* at this period of the year (which are considered as red picoeucaryotes by flow
645 cytometry). In addition, among the cryptophytes, few genera exhibiting a wide size range (between 5
646 and 19 μ m) are commonly detected (Marie et al., 2010). Nanoeukaryotes are frequently represented by
647 Haptophytes, Stramenopiles and Chlorophytes. *Emiliana huxleyi* is always reported as the dominant
648 coccolithophore species and is known to bloom in the outer shelf of the WEC (Garcia-soto et al.,
649 1995). In addition, a high diversity of diatoms and dinoflagellates is also observed in the WEC (*e.g.*
650 Widdicombe et al., 2010). Such taxonomical diversity results also in size diversity which is related to
651 physiological traits (Litchman et al., 2010). Consequently, the pigment expression varies. Here, the
652 variations of the trait’s expression considering the three hypotheses (the plasticity and genetic
653 adaptation of the traits, the selection of the optimal traits under biological pressures and the lack of
654 taxonomical determination by automated “pulse shape-recording” flow cytometry) lead to changes in
655 related traits such as nutrient uptake, cell carbon and nitrogen content within each groups and between
656 the communities. The fact that traits such as the cell-size, abundance and total or per cell red
657 fluorescence per group differed significantly between communities, suggests optimum growth
658 conditions in the recorded abiotic parameters for their growth combined with trade-off in biological
659 pressure and variations of the taxonomical composition.

660 4.3 Environment vs. spatial variations

661 We expected a greater influence of environment over space structuring phytoplankton communities in
662 the English Channel. Indeed, abiotic filtering has been shown to play a key-role in shaping
663 phytoplankton assemblages (Cornwell and Ackerly, 2015). However, in the present study, variation
664 partitioning showed that variability in each community depended more on spatial (25 to 70%) than on
665 environmental (15% to 59%) variation within space inducing significantly the environmental
666 variations (16% to 46%; Table 2). Despite heterogeneity is well reported in other areas and seas
667 (Bonato et al., 2015; Marrec et al., 2018; Thyssen et al., 2015), our study allowed quantifying the
668 importance of space and environment on high frequency flow cytometry. Here, the spatiotemporal
669 study of the phytoplankton communities showed an imbalance between groups over one location, this
670 means that high abundance of a group coincided with low abundance of another group and vice-versa.
671 For example, the highest abundance of Coccolithophore-like cells was observed out of the English
672 Channel, in the Celtic Seas shelf where none of the other groups (except *Synechococcus*-like cells)
673 exhibited highest abundance (Fig. 5). This was observed also for both picoeukaryote groups, the
674 highest abundance of the PicoLowFLR was found where PicoHighFLR abundance was relatively low
675 and vice-versa. NanoLowFLR and NanoHighFLR showed the same trend. As previously shown with
676 temperature and vertical stability, each group might result of the selection by a combination of the
677 best conditions (environmental, physical and biotic interactions) for their growth, metabolism and
678 access to resources thus defining their ecological niche (Margalef, 1978; Reynolds, 2006, 1994, 1984;
679 Tilman et al., 1982). Despite *Synechococcus*-like cells share the same environmental niche as
680 picoeukaryotes (Chen et al., 2011), we could identify some spot of exclusion on both sides near the
681 Ushant front between *Synechococcus*-like cells and PicoLowFLR and others between *Synechococcus*-
682 like cells and PicoHighFLR which are consistent either with sharing niche (Chen et al., 2011) either
683 with exclusions (Winder, 2009). However, both studies considered only one picoeukaryotes group and
684 analyzed discrete samples while we could characterize at a high spatial and/or temporal resolution two
685 sub-groups in the picoeukaryotes and *Synechococcus*-like cells. Consequently, the characterization of
686 sub-groups may increase the ecological understanding of plankton functional groups. As previously
687 discussed, phytoplankton traits are also known to partition ecological niche of species or functional
688 groups (Litchman et al., 2010; Litchman and Klausmeier, 2008). Therefore, by extension, cytometry-

689 derived traits (Fragoso et al., 2019; Malkassian et al., 2011; Pomati et al., 2011; Pomati and Nizzetto,
690 2013) are important to be taken into account when considering the spatial and/or temporal ecological
691 niche of the functional groups.

692 **4.4 Spatial structure analysis**

693 Based on the Mantel correlograms (Fig. 10), phytoplankton communities are autocorrelated from
694 small to large scale (20 km to 110 km), depending on the communities. The highest correlation at
695 nearer distance followed by the decrease in autocorrelation define a stronger structure for closer
696 sampled units. Due to the high spatial resolution between two sampling units (*i.e.* 3.4 km), we state
697 phytoplankton communities to be structured at the sub-mesoscale (1 – 10 km). The local structuration
698 is also supported by the maps of each phytoplankton group (Fig. 5), their distribution with respect to
699 the Ushant front (Fig. 6) and the coefficient of variation (Table 2), which highlighted heterogeneity
700 and sharp shifts of total abundance, confirming a local structuration. This measure on the field was
701 congruent with previous findings using conventional flow cytometry (Martin et al., 2005), remote
702 sensing (d'Ovidio et al., 2010) and modelling (Lévy et al., 2014; Mahadevan et al., 2012). The
703 positive autocorrelation found for each community reflects the size of the patches for communities.
704 Several physical processes are well reported to generate patchiness. Small scale turbulence are well-
705 known to generate patchiness which can concentrate particles and phytoplankton at very small scales
706 (Schmitt and Seuront, 2008). Indeed, Pingree (Pingree, 1980; Pingree and Griffiths, 1978) noticed that
707 the English Channel is characterised by small turbulent and persistent eddies. Because phytoplankton
708 moves passively due to the movements of the fluids, eddies can generate patchiness of phytoplankton
709 and spatial heterogeneity. This is commonly observed in the North Atlantic Ocean in the Western
710 English Channel and the Bay of Seine (Mahadevan et al., 2012; Ménesguen and Gohin, 2006; Pingree
711 et al., 1978; Salomon and Breton, 1993) as in our study, despite we could not observe the eddies. In
712 the meanwhile, eddies contribute locally to water masses motion, changing the abiotic conditions
713 which allow a niche specialization (d'Ovidio et al., 2010). The association of the front in the Western
714 English Channel and the eddies frequently reported in the area are described to generate sub-
715 mesoscale turbulence (*i.e.* 1 – 10 km; Bracco et al., 2000; Perruche et al., 2011). This latter and the

716 passive transport of phytoplankton cause the important dispersal rates of phytoplankton (Lévy et al.,
717 2014). In our study, figure 4D defined the position of the fronts during the cruise and the figure 6
718 showed the distribution of each cytometric group with respect to the inner front. The dispersal rates
719 reflected here the heterogeneity in abundance around the front. Moreover, the English Channel is
720 highly hydrodynamical, exhibiting a heterogeneity between French and English coasts, Bay of Seine
721 and offshore waters in the strength of the tidal stream. This component also induces the strength of the
722 dispersal rate. Finally, high variability in each group's traits, inside each community, may also result
723 in the spatial variation of the strength of the dispersal, which increased the plasticity (Sultan and
724 Spencer, 2002; Via and Lande, 1985) thus the variability of their traits (Litchman et al., 2010).

725 **5. Conclusion**

726 In the present study, six phytoplankton communities were characterised based on the contribution of
727 each of the eight defined cytometric groups and their optical features and signatures, total abundance
728 and chlorophyll content. These optical features can be, to some extent, associated to life traits, from
729 coastal to offshore waters, where long term regular monitoring does not exist. Phytoplankton and their
730 derived traits were strongly dependent on the hydrology but, most of the times, the communities were
731 even more structured by the spatial descriptors. They include parameters which are not taken into
732 account in the environmental part such as positive and negative biological interactions, other
733 unmeasured environmental parameters, physical processes. Mantel correlogram made possible to
734 identify phytoplankton communities' variations at the sub-mesoscale (1 – 10 km) in the English
735 Channel. Physical parameters were proposed to explain these variabilities, by structuring the
736 hydrology (different water masses) as well as phytoplankton communities, which were not always
737 associated to a single water mass. Further work should investigate the traits responses to the
738 environmental conditions by applying high frequency flow cytometry in a regular basis, if possible,
739 connected to automated hydrological and biogeochemical measurements at high frequency, on a
740 seasonal and interannual basis. We could therefore define an extended phytoplankton typology within
741 the English Channel including all size classes and also their corresponding traits. This work requires
742 analysing data from the three tables (species or functional groups, environment and traits) and have

743 already been proposed for automated flow cytometry in previous studies (Breton et al., 2017; Fragoso
744 et al., 2019; Pomati et al., 2013) and should be generalized from individuals to the community level.

745 **Acknowledgments**

746 This work was carried out in the frame of the M.Sc. FOGEM (Université du Littoral-Côte d'Opale and
747 Université of Lille) internship co-funded by the Laboratory of Oceanology and Geosciences and the
748 "Pôle Environnement, Milieux Littoraux et Marins" of ULCO. At present Arnaud Louchart benefits of
749 a PhD grant of the Université du Littoral-Côte d'Opale and the French Region « Hauts-de-France ».
750 The CAMANOC cruise was funded by the DFF project. We would like to thank Morgane Travers, P.I.
751 of the CAMANOC cruise, the scientists involved, as well as the Captain and the crew of the R/V
752 Thalassa (IFREMER).

753 **References**

- 754 Alpine, A.E., Cloern, J.E., 1988. Phytoplankton growth rates in a light-limited environment, San
755 Francisco Bay. *Mar. Ecol. Prog. Ser.* 44, 167–173.
- 756 Álvarez, E., Nogueira, E., López-Urrutia, Á., 2017. In Vivo Single-Cell Fluorescence and Size
757 Scaling of Phytoplankton Chlorophyll Content . *Appl. Environ. Microbiol.* 83, 1–16.
758 <https://doi.org/10.1128/aem.03317-16>
- 759 Bentley, D., Hart, V., Guary, J.C., Statham, P.J., 1999. Dissolved nutrient distributions in the Central
760 English Channel. *Cont. Shelf Res.* 19. [https://doi.org/10.1016/S0278-4343\(99\)00054-0](https://doi.org/10.1016/S0278-4343(99)00054-0)
- 761 Bergquist, A.M., Carpenter, S.R., Latino, J.C., 1985. Shifts in phytoplankton size structure and
762 community composition during grazing by contrasting zooplankton assemblages. *Limnol.*
763 *Oceanogr.* 30, 1037–1045.
- 764 Bonato, S., Breton, E., Didry, M., Lizon, F., Cornille, V., Lécuyer, E., Christaki, U., Artigas, L.F.,
765 2016. Spatio-temporal patterns in phytoplankton assemblages in inshore-offshore gradients using
766 flow cytometry: A case study in the eastern English Channel. *J. Mar. Syst.* 156, 76–85.
767 <https://doi.org/10.1016/j.jmarsys.2015.11.009>
- 768 Bonato, S., Christaki, U., Lefebvre, A., Lizon, F., Thyssen, M., Artigas, L.F., 2015. High spatial
769 variability of phytoplankton assessed by flow cytometry, in a dynamic productive coastal area, in
770 spring: The eastern English Channel. *Estuar. Coast. Shelf Sci.* 154, 214–223.
771 <https://doi.org/10.1016/j.ecss.2014.12.037>
- 772 Borcard, D., Legendre, P., 2002. All-scale spatial analysis of ecological data by means of principal
773 coordinates of neighbour matrices. *Ecol. Modell.* 153, 51–68.
774 <https://doi.org/10.1016/j.catena.2016.01.006>
- 775 Bracco, A., Provenzale, A., Scheuring, I., 2000. Mesoscale vortices and the paradox of the plankton.
776 *Proc. R. Soc. B Biol. Sci.* 267, 1795–1800. <https://doi.org/10.1002/lipi.19660680811>
- 777 Breton, E., Christaki, U., Bonato, S., Didry, M., Artigas, L.F., 2017. Functional trait variation and

- 778 nitrogen use efficiency in temperate coastal phytoplankton. *Mar. Ecol. Prog. Ser.* 563, 35–49.
779 <https://doi.org/10.3354/meps11974>
- 780 Brylinski, J.M., Lagadeuc, Y., 1990. L'interface eaux côtières/eaux du large dans le Pas-de-Calais
781 (côte française) : une zone frontale. *Comptes rendus l'Académie des Sci.* 311, 535–540.
- 782 Charria, G., Lamouroux, J., De Mey, P., 2016. Optimizing observational networks combining gliders,
783 moored buoys and FerryBox in the Bay of Biscay and English Channel. *J. Mar. Syst.* 162, 112–
784 125. <https://doi.org/10.1016/j.jmarsys.2016.04.003>
- 785 Chen, B., Wang, L., Song, S., Huang, B., Sun, J., Liu, H., 2011. Comparisons of picophytoplankton
786 abundance, size, and fluorescence between summer and winter in northern South China Sea.
787 *Cont. Shelf Res.* 31, 1527–1540. <https://doi.org/10.1016/j.csr.2011.06.018>
- 788 Collier, J.L., 2000. Flow cytometry and the single cell in phycology. *J. Phycol.* 36, 628–644.
789 <https://doi.org/10.1046/j.1529-8817.2000.99215.x>
- 790 Cornwell, W.K., Ackerly, D.D., 2015. Community Assembly and Shifts in Plant Trait Distributions
791 across an Environmental Gradient in Coastal California Published by : Ecological Society of
792 America Community across an environmental in plant trait distributions assembly and shifts
793 gradient and. *Ecol. Monogr.* 79, 109–126. <https://doi.org/10.1890/07-1134.1>
- 794 Cullen, J., Ciotti, A., Davis, R., Lewis, M., 1997. Emerging technologies and modeling. *Limnol.*
795 *Oceanogr.* 42, 1223–1239.
- 796 d'Ovidio, F., De Monte, S., Alvain, S., Dandonneau, Y., Levy, M., 2010. Fluid dynamical niches of
797 phytoplankton types. *Proc. Natl. Acad. Sci.* 107, 18366–18370.
798 <https://doi.org/10.1073/pnas.1004620107>
- 799 De Monte, S., Soccodato, A., Alvain, S., D'Ovidio, F., 2013. Can we detect oceanic biodiversity
800 hotspots from space? *ISME J.* 7, 2054–2056. <https://doi.org/10.1038/ismej.2013.72>
- 801 Dubelaar, G.B.J., Geerders, P.J.F., Jonker, R.R., 2004. High frequency monitoring reveals
802 phytoplankton dynamics. *J. Environ. Monit.* 6, 946–952. <https://doi.org/10.1039/b409350j>
- 803 Dubelaar, G.B.J., Gerritzen, P.L., Beeker, A.E.R., Jonker, R.R., Tangen, K., 1999. Design and first
804 results of CytoBuoy: A wireless flow cytometer for in situ analysis of marine and fresh waters.
805 *Cytometry* 37, 247–254.
- 806 Edwards, M., Reid, P., Planque, B., 2001. Long-term and regional variability of phytoplankton
807 biomass in the Northeast Atlantic (1960-1995). *ICES J. Mar. Sci.* 58, 39–49.
808 <https://doi.org/10.1006/jmsc.2000.0987>
- 809 Eloire, D., Somerfield, P.J., Conway, D.V.P., Halsband-Lenk, C., Harris, R., Bonnet, D., 2010.
810 Temporal variability and community composition of zooplankton at station L4 in the Western
811 Channel: 20 years of sampling. *J. Plankton Res.* 32, 657–679.
812 <https://doi.org/10.1093/plankt/fbq009>
- 813 Falkowski, P.G., 1994. The role of phytoplankton photosynthesis in global biogeochemical cycles.
814 *Photosynth. Res.* 39, 235–258. <https://doi.org/10.1007/BF00014586>
- 815 Falkowski, P.G., Barber, R.T., Smetacek, V., 1998. Biogeochemical Controls and Feedbacks on Ocean
816 Primary Production. *Science (80-.)*. 281, 200–206. <https://doi.org/10.1126/science.281.5374.200>
- 817 Falkowski, P.G., Laws, E.A., Barber, R.T., Murray, J.W., 2003. Phytoplankton and Their Role in
818 Primary, New, and Export Production, in: *Ocean Biogeochemistry*. pp. 99–121.
819 https://doi.org/10.1007/978-3-642-55844-3_5

- 820 Field, C.B., Behrenfeld, M.J., Randerson, J.T., Falkowski, P., 1998. Primary production of the
821 biosphere: Integrating terrestrial and oceanic components. *Science* (80-). 281, 237–240.
822 <https://doi.org/10.1126/science.281.5374.237>
- 823 Foulon, E., Not, F., Jalabert, F., Cariou, T., Massana, R., Simon, N., 2008. Ecological niche
824 partitioning in the picoplanktonic green alga *Micromonas pusilla*: Evidence from environmental
825 surveys using phylogenetic probes. *Environ. Microbiol.* 10, 2433–2443.
826 <https://doi.org/10.1111/j.1462-2920.2008.01673.x>
- 827 Fragoso, G.M., Poulton, A.J., Pratt, N., Johnsen, G., Purdie, D.A., 2019. Trait-based analysis of
828 subpolar North Atlantic phytoplankton and plastidic ciliate communities using automated flow
829 cytometer. *Limnol. Oceanogr.* 64, 1–16. <https://doi.org/10.1002/lno.11189>
- 830 Garcia-soto, C., Fernández, E., Pingree, R.D., Harbour, D.S., 1995. Evolution and structure of a shelf
831 coccolithophore bloom in the western English channel. *J. Plankton Res.* 17, 2011–2036.
832 <https://doi.org/10.1093/plankt/17.11.2011>
- 833 Garcia-Soto, C., Pingree, R.D., 2009. Spring and summer blooms of phytoplankton
834 (SeaWiFS/MODIS) along a ferry line in the Bay of Biscay and western English Channel. *Cont.*
835 *Shelf Res.* 29, 1111–1122. <https://doi.org/10.1016/j.csr.2008.12.012>
- 836 Goberville, E., Beaugrand, G., Sautour, B., Tréguer, P., 2010. Climate-driven changes in coastal
837 marine systems of western Europe. *Mar. Ecol. Prog. Ser.* 408, 129–147.
838 <https://doi.org/10.3354/meps08564>
- 839 Gregg, W.W., Conkright, M.E., Ginoux, P., O'Reilly, J.E., Casey, N.W., 2003. Ocean primary
840 production and climate: Global decadal changes. *Geophys. Res. Lett.* 30, 10–13.
841 <https://doi.org/10.1029/2003GL016889>
- 842 Haraguchi, L., Jakobsen, H.H., Lundholm, N., Carstensen, J., 2017. Monitoring natural phytoplankton
843 communities: A comparison between traditional methods and pulse-shape recording flow
844 cytometry. *Aquat. Microb. Ecol.* 80, 77–92. <https://doi.org/10.3354/ame01842>
- 845 Hoch, T., Garreau, P., 1998. Phytoplankton dynamics in the english channel: A simplified three-
846 dimensional approach. *J. Mar. Syst.* 16, 133–150. [https://doi.org/10.1016/S0924-7963\(97\)00103-](https://doi.org/10.1016/S0924-7963(97)00103-6)
847 6
- 848 Holligan, P.M., Harbour, D.S., 1977. The vertical distribution and succession of phytoplankton in the
849 mwestern english channel in 1975 and 1976. *J. Mar. Biol. Assoc. United Kingdom* 57, 1075–
850 1093. <https://doi.org/10.1017/S002531540002614X>
- 851 Hydes, D.J., Wright, P.N., 1999. SONUS: The southern nutrients study 1995-1997. Rep. Southampt.
852 Oceanogr. Cent.
- 853 Iriarte, A., Purdie, D.A., 2004. Factors controlling the timing of major spring bloom events in an UK
854 south coast estuary. *Estuar. Coast. Shelf Sci.* 61, 679–690.
855 <https://doi.org/10.1016/j.ecss.2004.08.002>
- 856 Jouenne, F., Lefebvre, S., Véron, B., Lagadeuc, Y., 2007. Phytoplankton community structure and
857 primary production in small intertidal estuarine-bay ecosystem (eastern English Channel,
858 France). *Mar. Biol.* 151, 805–825. <https://doi.org/10.1007/s00227-006-0440-z>
- 859 Karp-Boss, L., Boss, E., Jumars P.A., 1996. Nutrient Fluxes to Planktonic Osmotrophs in the Presence
860 of Fluid Motion. *Oceanogr. Mar. Biol. an Annu. Rev.* 34, 71–107.
- 861 Kifle, D., Purdie, D.A., 1993. The seasonal abundance of the phototrophic ciliate *Mesodinium rubrum*
862 in Southempton water, England. *J. Plankton Res.* 5, 823–833.

- 863 Lampert, W., Fleckner, W., Rai, H., Taylor, B.E., 1986. Phytoplankton control by grazing
864 zooplankton: A study on the spring clear water phase. *Limnol. Oceanogr.* 31, 478–490.
865 <https://doi.org/10.4319/lo.1986.31.3.0478>
- 866 Landeira, J.M., Ferron, B., Lunven, M., Morin, P., Marie, L., Sourisseau, M., 2014. Biophysical
867 interactions control the size and abundance of large phytoplankton chains at the ushant tidal
868 front. *PLoS One* 9, e90507. <https://doi.org/10.1371/journal.pone.0090507>
- 869 Leakey, R.J.G., Burkill, P.H., Sleight, M.A., 1992. Planktonic ciliates in Southampton Water:
870 abundance, biomass, production, and role in pelagic carbon flow. *Mar. Biol.* 114, 67–83.
871 <https://doi.org/10.1038/470444a>
- 872 Lefebvre, A., Poisson-Caillault, E., 2019. High resolution overview of phytoplankton spectral groups
873 and hydrological conditions in the eastern English Channel using unsupervised clustering. *Mar.*
874 *Ecol. Prog. Ser.* 608, 73–92. <https://doi.org/https://doi.org/10.3354/meps12781>
- 875 Legendre, P., Legendre, L., 1998. Numerical ecology. 2nd. Elsevier Sci.
876 <https://doi.org/10.1017/CBO9781107415324.004>
- 877 Lévy, M., Jahn, O., Dutkiewicz, S., Follows, M.J., 2014. Phytoplankton diversity and community
878 structure affected by oceanic dispersal and mesoscale turbulence. *Limnol. Oceanogr. Fluids*
879 *Environ.* 4, 67–84. <https://doi.org/10.1215/21573689-2768549>
- 880 Litchman, E., 2007. Resource Competition and the Ecological Success of Phytoplankton, in:
881 Falkowski, P.G., Knoll, A.H. (Eds.), *Evolution of Primary Producers in the Sea*. Academic Press,
882 pp. 351–375. <https://doi.org/https://doi.org/10.1016/B978-0-12-370518-1.X5000-0>
- 883 Litchman, E., de Tezanos Pinto, P., Klausmeier, C.A., Thomas, M.K., Yoshiyama, K., 2010. Linking
884 traits to species diversity and community structure in phytoplankton. *Hydrobiologia* 653, 15–28.
885 <https://doi.org/10.1007/s10750-010-0341-5>
- 886 Litchman, E., Klausmeier, C.A., 2008. Trait-Based Community Ecology of Phytoplankton. *Annu.*
887 *Rev. Ecol. Syst.* 39, 615–639. <https://doi.org/10.1146/annurev.ecolsys.39.110707.173549>
- 888 Litchman, E., Klausmeier, C.A., Schofield, O.M., Falkowski, P.G., 2007. The role of functional traits
889 and trade-offs in structuring phytoplankton communities: Scaling from cellular to ecosystem
890 level. *Ecol. Lett.* 10, 1170–1181. <https://doi.org/10.1111/j.1461-0248.2007.01117.x>
- 891 Litchman, E., Klausmeier, C.A., Yoshiyama, K., 2009. Contrasting size evolution in marine and
892 freshwater diatoms. *Proc. Natl. Acad. Sci.* 106, 2665–2670.
893 <https://doi.org/10.1073/pnas.0810891106>
- 894 Mahadevan, A., D'Asaro, E., Lee, C., Perry, M.J., 2012. Eddy-Driven Stratification Initiates North
895 Atlantic Spring Phytoplankton Blooms. *Science (80-.)*. 337, 54–58.
- 896 Malkasian, A., Nerini, D., Van Dijk, M.A., Thyssen, M., Mante, C., Gregori, G., 2011. Functional
897 analysis and classification of phytoplankton based on data from an automated flow cytometer.
898 *Cytom. Part A* 79 A, 263–275. <https://doi.org/10.1002/cyto.a.21035>
- 899 Marañón, E., 2015. Cell Size as a Key Determinant of Phytoplankton Metabolism and Community
900 Structure. *Ann. Rev. Mar. Sci.* 7, 241–264. <https://doi.org/10.1146/annurev-marine-010814-015955>
- 902 Margalef, R., 1978. Life-forms of phytoplankton as survival alternative in an unstable environment.
903 *Oceanologica* 1, 493–509.
- 904 Marie, D., Shi, X.L., Rigaut-Jalabert, F., Vaultot, D., 2010. Use of flow cytometric sorting to better
905 assess the diversity of small photosynthetic eukaryotes in the English Channel. *FEMS Microbiol.*

- 906 Ecol. 72, 165–178. <https://doi.org/10.1111/j.1574-6941.2010.00842.x>
- 907 Marrec, P., Cariou, T., Collin, E., Durand, A., Latimier, M., Macé, E., Morin, P., Raimund, S., Vernet,
908 M., Bozec, Y., 2013. Seasonal and latitudinal variability of the CO₂ system in the western
909 English Channel based on Voluntary Observing Ship (VOS) measurements. *Mar. Chem.* 155,
910 29–41. <https://doi.org/10.1016/j.marchem.2013.05.014>
- 911 Marrec, P., Cariou, T., Latimier, M., Macé, E., Morin, P., Vernet, M., Bozec, Y., 2014. Spatio-
912 temporal dynamics of biogeochemical processes and air – sea CO₂ fluxes in the Western
913 English Channel based on two years of FerryBox deployment. *J. Mar. Syst.* 140, 26–38.
914 <https://doi.org/10.1016/j.jmarsys.2014.05.010>
- 915 Marrec, P., Doglioli, A.M., Grégori, G., Dugenne, M., Della Penna, A., Bhairy, N., Cariou, T., Hélias
916 Nunige, S., Lahbib, S., Rougier, G., Wagener, T., Thyssen, M., 2018. Coupling physics and
917 biogeochemistry thanks to high-resolution observations of the phytoplankton community
918 structure in the northwestern Mediterranean Sea. *Biogeosciences* 15, 1579–1606.
919 <https://doi.org/10.5194/bg-15-1579-2018>
- 920 Martin, A.P., Zubkov, M. V., Burkill, P.H., Holland, R.J., 2005. Extreme spatial variability in marine
921 picoplankton and its consequences for interpreting Eulerian time-series. *Biol. Lett.* 1, 366–369.
922 <https://doi.org/10.1098/rsbl.2005.0316>
- 923 Ménesguen, A., Gohin, F., 2006. Observation and modelling of natural retention structures in the
924 English Channel. *J. Mar. Syst.* 63, 244–256. <https://doi.org/10.1016/j.jmarsys.2006.05.004>
- 925 Menesguen, A., Hoch, T., 1997. Modelling the biogeochemical cycles of elements limiting primary
926 production in the English Channel. I. Role of thermohaline stratification. *Mar. Ecol. Prog. Ser.*
927 146, 173–188.
- 928 Millie, D.F., Schofield, O.M., Kirkpatrick, G.J., Johnsen, G., Tester, P.A., Vinyard, B.T., 1997.
929 Detection of harmful algal blooms using photopigments and absorption signatures: A case study
930 of the Florida red tide dinoflagellate, *Gymnodinium breve*. *Limnol. Oceanogr.* 42, 1240–1251.
- 931 Napoléon, C., Fiant, L., Raimbault, V., Claquin, P., 2013. Study of dynamics of phytoplankton and
932 photosynthetic parameters using opportunity ships in the western English Channel. *J. Mar. Syst.*
933 128, 146–158. <https://doi.org/10.1016/j.jmarsys.2013.04.019>
- 934 Napoléon, C., Fiant, L., Raimbault, V., Riou, P., Claquin, P., 2014. Dynamics of phytoplankton
935 diversity structure and primary productivity in the English Channel. *Mar. Ecol. Prog. Ser.* 505,
936 49–64. <https://doi.org/10.3354/meps10772>
- 937 Napoléon, C., Raimbault, V., Fiant, L., Riou, P., Lefebvre, S., Lampert, L., Claquin, P., 2012.
938 Spatiotemporal dynamics of physicochemical and photosynthetic parameters in the central
939 English Channel. *J. Sea Res.* 69, 43–52. <https://doi.org/10.1016/j.seares.2012.01.005>
- 940 Not, F., Latasa, M., Marie, D., Cariou, T., Vaultot, D., Simon, N., 2004. A Single Species, *Micromonas*
941 *pusilla* (Prasinophyceae), Dominates the Eukaryotic Picoplankton in the Western English
942 Channel. *Appl. Environ. Microbiol.* 70, 4064–4072. <https://doi.org/10.1128/AEM.70.7.4064>
- 943 Pannard, A., Claquin, P., Klein, C., Le Roy, B., Véron, B., 2008. Short-term variability of the
944 phytoplankton community in coastal ecosystem in response to physical and chemical conditions '
945 changes. *Estuar. Coast. Shelf Sci.* 80, 212–224. <https://doi.org/10.1016/j.ecss.2008.08.008>
- 946 Pearl, H.W., Valdes-Weaver, L.M., Joyner, A.R., Winkelmann, V., 2007. Phytoplankton indicators of
947 ecological change in the eutrophying Pamlico sound system, North Carolina. *Ecol. Appl.* 17, 88–
948 101.
- 949 Perruche, C., Pondaven, P., Lapeyre, G., Rivière, P., Carton, X., 2011. Effects of surface quasi-

- 950 geostrophic turbulence on phytoplankton competition and coexistence. *J. Mar. Res.* 69, 105–135.
951 <https://doi.org/10.1357/002224011798147606>
- 952 Pingree, R.D., 1980. *Physical Oceanography of the Celtic Sea and English Channel*. Elsevier
953 *Oceanogr. Ser.* 24, 415–465. [https://doi.org/10.1016/S0422-9894\(08\)71358-8](https://doi.org/10.1016/S0422-9894(08)71358-8)
- 954 Pingree, R.D., Griffiths, D.K.G., 1978. Tidal Fronts on the Shelf Seas Around the British Isles Marine
955 Biological Association of the United Kingdom, Plymouth, England. *J. Geophys. Res. Ocean.* 83,
956 4615–4622. <https://doi.org/10.1029/JC083iC09p04615>
- 957 Pingree, R.D., Holligan, P.M., Head, R.N., 1977. Survival of dinoflagellates blooms in the western
958 English Channel. *Nature* 265, 266–269. <https://doi.org/10.1038/266309a0>
- 959 Pingree, R.D., Holligan, P.M., Mardell, G.T., 1979. Phytoplankton growth and cyclonic eddies. *Nature*
960 278, 245–247.
- 961 Pingree, R.D., Holligan, P.M., Mardell, G.T., 1978. The effects of vertical stability on phytoplankton
962 distributions in the summer on the northwest European Shelf. *Deep-Sea Res.* 25, 1011–1028.
963 [https://doi.org/10.1016/0146-6291\(78\)90584-2](https://doi.org/10.1016/0146-6291(78)90584-2)
- 964 Pingree, R.D., Pugh, P.R., Holligan, P.M., Forster, G.R., 1975. Summer phytoplankton blooms and red
965 tides along tidal fronts in the approaches to the English Channel. *Nature* 258, 672–677.
966 <https://doi.org/10.1038/253600a0>
- 967 Pomati, F., Jokela, J., Simona, M., Veronesi, M., Ibelings, B.W., 2011. An automated platform for
968 phytoplankton ecology and aquatic ecosystem monitoring. *Environ. Sci. Technol.* 45, 9658–
969 9665. <https://doi.org/10.1021/es201934n>
- 970 Pomati, F., Kraft, N.J.B., Posch, T., Eugster, B., Jokela, J., Ibelings, B.W., 2013. Individual Cell
971 Based Traits Obtained by Scanning Flow-Cytometry Show Selection by Biotic and Abiotic
972 Environmental Factors during a Phytoplankton Spring Bloom. *PLoS One* 8.
973 <https://doi.org/10.1371/journal.pone.0071677>
- 974 Pomati, F., Nizzetto, L., 2013. Assessing triclosan-induced ecological and trans-generational effects in
975 natural phytoplankton communities: A trait-based field method. *Ecotoxicology* 22, 779–794.
976 <https://doi.org/10.1007/s10646-013-1068-7>
- 977 Rantajärvi, E., Olsonen, R., Hällfors, S., Leppänen, J.M., Raateoja, M., 1998. Effect of sampling
978 frequency on detection of natural variability in phytoplankton: Unattended high-frequency
979 measurements on board ferries in the Baltic Sea. *ICES J. Mar. Sci.* 55, 697–704.
980 <https://doi.org/10.1006/jmsc.1998.0384>
- 981 Rassoulzadegan, F., Laval-Peuto, M., Sheldon, R.W., 1988. Partitioning of the food ration of marine
982 ciliates between pico- and nanoplankton. *Hydrobiologia* 159, 75–88.
983 <https://doi.org/10.1007/BF00007369>
- 984 Reynolds, C.S., 2006. *Ecology of Phytoplankton*, Cambridge. ed. Cambridge.
- 985 Reynolds, C.S., 1994. The long, the short and the stalled: on the attributes of phytoplankton selected
986 by physical mixing in lakes and rivers. *Hydrobiologia* 289, 9–21.
- 987 Reynolds, C.S., 1984. *The ecology of freshwater phytoplankton*. Cambridge University Press.
- 988 Ribalet, F., Marchetti, A., Hubbard, K.A., Brown, K., Durkin, C.A., Morales, R., Robert, M.,
989 Swalwell, J.E., Tortell, P.D., Armbrust, V.E., 2010. Unveiling a phytoplankton hotspot at a
990 narrow boundary between coastal and offshore waters. *Proc. Natl. Acad. Sci.* 107, 16571–16576.
991 <https://doi.org/10.1073/pnas.1005638107>

- 992 Richardson, T.L., Pinckney, J.L., 2004. Monitoring of the toxic dinoflagellate *Karenia brevis* using
993 gyroxanthin-based detection methods. *J. Appl. Phycol.* 16, 315–328.
994 <https://doi.org/10.1023/B:JAPH.0000047788.31312.4f>
- 995 Rutten, T.P.A., Sandee, B., Hofman, A.R.T., 2005. Phytoplankton monitoring by high performance
996 flow cytometry: A successful approach? *Cytom. Part A* 64, 16–26.
997 <https://doi.org/10.1002/cyto.a.20106>
- 998 Salomon, J., Breton, M., 1993. An atlas of long-term currents in the Channel. *Oceanol. acta* 16, 439–
999 448.
- 1000 Schmitt, F.G., Seuront, L., 2008. Intermittent turbulence and copepod dynamics: Increase in encounter
1001 rates through preferential concentration. *J. Mar. Syst.* 70, 263–272.
1002 <https://doi.org/10.1016/j.jmarsys.2007.01.008>
- 1003 Schubert, A., Telcs, A., 2014. A note on the Jaccardized Czekanowski similarity index. *Scientometrics*
1004 98, 1397–1399. <https://doi.org/10.1007/s11192-013-1044-2>
- 1005 Simpson, J.H., Nunes, R.A., 1981. The tidal intrusion front: An estuarine convergence zone. *Estuar.
1006 Coast. Shelf Sci.* 13. [https://doi.org/10.1016/S0302-3524\(81\)80024-2](https://doi.org/10.1016/S0302-3524(81)80024-2)
- 1007 Smyth, T.J., Fishwick, J.R., Al-Moosawi, L., Cummings, D.G., Harris, C., Kitidis, V., Rees, A.,
1008 Martinez-Vicente, V., Woodward, E.M.S., 2010. A broad spatio-temporal view of the Western
1009 English Channel observatory. *J. Plankton Res.* 32, 585–601.
1010 <https://doi.org/10.1093/plankt/fbp128>
- 1011 Sournia, A., Birrien, J.L., Douvillé, J.L., Klein, B., Viollier, M., 1987. A daily study of the diatom
1012 spring bloom at Roscoff (France) in 1985. I. The spring bloom within the annual cycle. *Estuar.
1013 Coast. Shelf Sci.* 25, 355–367. [https://doi.org/10.1016/0272-7714\(87\)90078-3](https://doi.org/10.1016/0272-7714(87)90078-3)
- 1014 Sultan, S.E., Spencer, H.G., 2002. Metapopulation Structure Favors Plasticity over Local Adaptation.
1015 *Am. Nat.* 160, 271–283.
- 1016 Tarran, G.A., Bruun, J.T., 2015. Nanoplankton and picoplankton in the Western English Channel:
1017 Abundance and seasonality from 2007-2013. *Prog. Oceanogr.* 137, 446–455.
1018 <https://doi.org/10.1016/j.pocean.2015.04.024>
- 1019 Thorel, M., Claquin, P., Schapira, M., Le Gendre, R., Riou, P., Goux, D., Le Roy, B., Raimbault, V.,
1020 Deton-Cabanillas, A.F., Bazin, P., Kientz-Bouchart, V., Fauchot, J., 2017. Nutrient ratios
1021 influence variability in *Pseudo-nitzschia* species diversity and particulate domoic acid production
1022 in the Bay of Seine (France). *Harmful Algae* 68, 192–205.
1023 <https://doi.org/10.1016/j.hal.2017.07.005>
- 1024 Thyssen, M., Alvain, S., Lefèbvre, A., Dessailly, D., Rijkeboer, M., Guiselin, N., Creach, V., Artigas,
1025 L.F., 2015. High-resolution analysis of a North Sea phytoplankton community structure based on
1026 in situ flow cytometry observations and potential implication for remote sensing. *Biogeosciences*
1027 12, 4051–4066. <https://doi.org/10.5194/bg-12-4051-2015>
- 1028 Thyssen, M., Mathieu, D., Garcia, N., Denis, M., 2008a. Short-term variation of phytoplankton
1029 assemblages in Mediterranean coastal waters recorded with an automated submerged flow
1030 cytometer. *J. Plankton Res.* 30, 1027–1040. <https://doi.org/10.1093/plankt/fbn054>
- 1031 Thyssen, M., Tarran, G.A., Zubkov, M. V., Holland, R.J., Grégori, G., Burkill, P.H., Denis, M.,
1032 2008b. The emergence of automated high-frequency flow cytometry: Revealing temporal and
1033 spatial phytoplankton variability. *J. Plankton Res.* 30, 333–343.
1034 <https://doi.org/10.1093/plankt/fbn005>
- 1035 Tilman, D., Kilham, S.S., Kilham, P., 1982. Phytoplankton Community Ecology: The Role of

- 1036 Limiting Nutrients. *Annu. Rev. Ecol. Syst.* 13, 349–372.
- 1037 Travers-Trolet, M., Verin, Y., 2014. CAMANOC cruise, RV Thalassa.
1038 <https://doi.org/10.17600/14001900>
- 1039 Van Leeuwen, S., Tett, P., Mills, D., van der Molen, J., 2015. Stratified and nonstratified areas in the
1040 North Sea: Long-term variability and biological an policy implications. *J. Geophys. Res. Ocean.*
1041 120, 4670–4686. <https://doi.org/10.1002/2014JC010485>.Received
- 1042 Via, S., Lande, R., 1985. Genotype-Environment Interaction and the Evolution of Phenotypic
1043 Plasticity. *Evolution* (N. Y). 39, 505–522. <https://doi.org/10.2307/2408649>
- 1044 Violle, C., Navas, M.L., Vile, D., Kazakou, E., Fortunel, C., Hummel, I., Garnier, E., 2007. Let the
1045 concept of trait be functional! *Oikos* 116, 882–892. [https://doi.org/10.1111/j.0030-](https://doi.org/10.1111/j.0030-1299.2007.15559.x)
1046 [1299.2007.15559.x](https://doi.org/10.1111/j.0030-1299.2007.15559.x)
- 1047 Ward, J.H.J., 1963. Hierarchical grouping to optimize and objective function. *J. Am. Stat. Assoc.* 58,
1048 236–244. <https://doi.org/10.1080/01621459.1963.10500845>
- 1049 Widdicombe, C.E., Eloire, D., Harbour, D., Harris, R.P., Somerfield, P.J., 2010. Long-term
1050 phytoplankton community dynamics in the Western English Channel. *J. Plankton Res.* 32, 643–
1051 655. <https://doi.org/10.1093/plankt/fbp127>
- 1052 Winder, M., 2009. Photosynthetic picoplankton dynamics in Lake Tahoe: Temporal and spatial niche
1053 partitioning among prokaryotic and eukaryotic cells. *J. Plankton Res.* 31, 1307–1320.
1054 <https://doi.org/10.1093/plankt/fbp074>
- 1055

Highlights of manuscript CSR_2019_156

Automated flow cytometry addresses phytoplankton community changes at high frequency

Eight cytometric groups are characterized from pico- to microphytoplankton size range

Variation in cytometry-derived traits can be characterized between communities

Frontal structures drive phytoplankton spatial distribution at sub-mesoscale

Journal Pre-proof

Conflict of interest

The authors declare that they have no conflict of interest.

Journal Pre-proof